






## Article

# Assessment of Forest Fire Severity for a Management Conceptual Model: Case Study in Vilcabamba, Ecuador

Fernando González <sup>1</sup>, Fernando Morante-Carballo <sup>2,3,4</sup>, Aníbal González <sup>1</sup>, Lady Bravo-Montero <sup>2,\*</sup>, César Benavidez-Silva <sup>1</sup> and Fantina Tedim <sup>5</sup>

<sup>1</sup> Centro de Investigaciones Territoriales, Universidad Nacional de Loja (UNL), Ciudadela Universitaria Guillermo Falconí Espinosa, Loja 110101, Ecuador; fernando.gonzalez@unl.edu.ec (F.G.); anibal.gonzalez@unl.edu.ec (A.G.); cesar.benavidez@unl.edu.ec (C.B.-S.)

<sup>2</sup> Centro de Investigación y Proyectos Aplicados a las Ciencias de la Tierra (CIPAT), ESPOL Polytechnic University, Campus Gustavo Galindo, Km. 30.5 Vía Perimetral, Guayaquil 090902, Ecuador; fmorante@espol.edu.ec

<sup>3</sup> Facultad de Ciencias Naturales y Matemáticas (FCNM), ESPOL Polytechnic University, Campus Gustavo Galindo, Km. 30.5 Vía Perimetral, Guayaquil 090902, Ecuador

<sup>4</sup> Geo-Recursos y Aplicaciones (GIGA), ESPOL Polytechnic University, Campus Gustavo Galindo, Km. 30.5 Vía Perimetral, Guayaquil 090902, Ecuador

<sup>5</sup> Research Centre in Geography and Spatial Planning (CEGOT), Geography Department, Faculty of Arts and Humanities, University of Porto, Via Panorâmica, P.O. Box 4150-564 Porto, Portugal; ftedim@letras.up.pt

\* Correspondence: lkbravo@espol.edu.ec; Tel.: +593-95-914-1436

**Abstract:** Wildfires are affecting natural ecosystems worldwide, causing economic and human losses and exacerbated by climate change. Models of fire severity and fire susceptibility are crucial tools for fire monitoring. This case study analyses a fire event on 3 September 2019 in Vilcabamba parish, Loja province, Ecuador. This article aims to assess the severity and susceptibility of a fire through spectral indices and multi-criteria methods for establishing a fire action plan proposal. The methodology comprises the following: (i) the acquisition of Sentinel-2A products for the calculation of spectral indices; (ii) a fire severity model using differentiated indices (dNBR and dNDVI) and a fire susceptibility model using the Analytic Hierarchy Process (AHP) method; (iii) model validation using Logistic Regression (LR) and Non-metric Multidimensional Scaling (NMDS) algorithms; (iv) the proposal of an action plan for fire management. The Normalised Burn Ratio (NBR) index revealed that 10.98% of the fire perimeter has burned areas with moderate-high severity in post-fire scenes (2019) and decreased to 0.01% for post-fire scenes in 2021. The Normalised Difference Vegetation Index (NDVI) identified 67.28% of the fire perimeter with null photosynthetic activity in the post-fire scene (2019) and 5.88% in the post-fire scene (2021). The Normalised Difference Moisture Index (NDMI) applied in the pre-fire scene identified that 52.62% has low and dry vegetation (northeast), and 8.27% has high vegetation cover (southwest). The dNDVI identified 10.11% of unburned areas and 7.91% using the dNBR. The fire susceptibility model identified 11.44% of the fire perimeter with null fire susceptibility. These results evidence the vegetation recovery after two years of the fire event. The models demonstrated excellent performance for fire severity models and were a good fit for the AHP model. We used the Root Mean Square Error (RMSE) and area under the curve (AUC); dNBR and dNDVI have an RMSE of 0.006, and the AHP model has an RMSE of 0.032. The AUC = 1.0 for fire severity models and AUC = 0.6 for fire susceptibility. This study represents a holistic approach by combining Google Earth Engine (GEE), Geographic Information System (GIS), and remote sensing tools for proposing a fire action plan that supports decision making. This study provides escape routes that considered the most significant fire triggers, the AHP, and fire severity approaches for monitoring wildfires in Andean regions.

**Keywords:** remote sensing; forest fire susceptibility; decision making; Google Earth Engine; Geographic Information System; wildfires



**Citation:** González, F.; Morante-Carballo, F.; González, A.; Bravo-Montero, L.; Benavidez-Silva, C.; Tedim, F. Assessment of Forest Fire Severity for a Management Conceptual Model: Case Study in Vilcabamba, Ecuador. *Forests* **2024**, *15*, 2210. <https://doi.org/10.3390/f15122210>

Academic Editors: Rafael Coll Delgado and Rafael De Ávila Rodrigues

Received: 25 November 2024

Accepted: 10 December 2024

Published: 16 December 2024



**Copyright:** © 2024 by the authors. Licensee MDPI, Basel, Switzerland. This article is an open access article distributed under the terms and conditions of the Creative Commons Attribution (CC BY) license (<https://creativecommons.org/licenses/by/4.0/>).

## 1. Introduction

Global change includes increased temperatures and prolonged droughts, which create the ideal conditions for increasing the likelihood of spreading extreme forest fires [1]. Forests present microclimates that strongly contrast with the climate outside them. Integrating microclimates in ecological research will promote the better understanding of forests' biodiversity and functions related to climate and climate change [2]. A challenge in understanding the fire-prone landscapes is their approach as coupled human and natural systems [3]. Anthropogenic activities, such as those in the recreational and agricultural sectors and human settlements, are associated with high wildfire risk [4]. For example, farmers consider burning essential for clearing vegetation or weeds, reducing acidity, and nutrient availability [5]. However, in high-intensity fires, these burning practises in agriculture affect microfauna, evapotranspiration, the reproduction of plant species, nutrients, and soil fertility [6].

Extreme wildfires are highly destructive agents within the ecosystem that impact the environment, wildlife habitats, and surrounding communities [7]. Moreover, wildfires destroy trees, shrubs, and other vegetation types, leaving the area barren, and changing hydrological processes (i.e., infiltration, interception) [8]. Wildfires can release large amounts of smoke and other pollutants into the air, causing health problems for humans and animals [9]. The intense heat caused by wildfires alters the chemical and physical properties of the soil, making it less fertile and unable to support plant growth [10].

Worldwide, recorded fires over time affect numerous ecosystems. For instance, in 2018, Washington, Oregon, Idaho, Nevada, and California recorded a burned area of 4000 hectares (ha) and 100 deaths [11]. Meanwhile, the Australian mega-fires in 2019 originated from natural conditions, consumed 70,000 ha. and affected regions such as Queensland, New South Wales, Victoria, and Tasmania [12]. The mega-fires of 2017 occurred in Pedrógão Grande (Portugal) and Gois, causing 64 deaths, with 200 individuals sustaining injuries and leaving a burned area of 45,000 ha [13]. In a local context, the Loja canton in Ecuador has experienced several forest fires, with a burned area of 12,848 ha from 2010 to 2022 [14].

In Ecuador, fires are mainly widespread during the dry season (from June to September), because solar radiation increases and produces hydric stress in vegetation and dried soil and lowers precipitation [15]. The leading causes of wildfires in this country are human activities, such as agricultural burning, campfires, and discarded cigarette butts, as well as the effects of climate change, which are leading to drier and hotter conditions [16]. The case study of this article comprises Vilcabamba parish in Loja Province in Ecuador, an Andean region in altitudes over the 1400 m.a.s.l. [17].

Remote sensing tools are widely used to understand wildfire dynamics. However, these techniques present some limitations due to weather conditions associated with cloud cover, which are challenges with observations on terrestrial surfaces [18]. However, multi-temporal analysis and machine learning based on remote sensing and statistical analysis (i.e., Logistic Regression, Multivariate Adaptive Regression Spline, Random Forest) facilitates the understanding of spatial, social dynamics and the temporality of fire events on the land surface [19]. The time series data of spectral indices could be inconvenienced due to cloudiness, aerosols, sun, ozone, and dust [20]. In this way, the application of the Cloud-gap-filled (CGF) method through Google Earth Engine (GEE) allows for efficient cloud removal, especially in Andean regions with high cloud cover [21].

Spectral indices qualify the phenological behaviour of plant species, showing their vigour, development, and dynamics [22]. The Normalised Difference Vegetation Index (NDVI) is used for the analysis of vegetation recovery, photosynthetic activity, mapping fire severity, crop yields, climate change, drought mapping, and the impact of flooding on crops [23,24]. The Normalised Burn Ratio (NBR) is one of the most used indices to assess fire severity, and its primary function is the detection of burned areas and vegetation status [25].

This study focuses on the need to understand and prevent the effects of forest fires, a phenomenon that represents a critical threat to ecosystems, biodiversity and human

communities. Fire severity levels provide a fundamental perspective for assessing environmental impact while developing susceptibility models to identify fire-prone areas. However, in Vilcabamba parish, there is no evidence of studies that analyse the severity of fires or government reports documenting the scars these events left. Likewise, no multi-criteria model has been developed to identify areas susceptible to forest fires. The available scientific literature is limited to quantifying fire frequency [14]. Additionally, forest fire monitoring usually includes the application of quantitative techniques based on remote sensing tools, statistical algorithms or machine learning methods. However, a holistic approach considering both qualitative and quantitative approaches is needed for a better explanation of fire events and successfully establishing an action plan oriented to support decision-making processes. Therefore, the research question of this study is as follows: How does assessing fire severity and susceptibility contribute to establishing a proposed action plan for fire monitoring and prevention?

The aim of this study is to assess the severity and the susceptibility of a fire event in Vilcabamba parish by calculating spectral indices such as the NDVI, NBR, and Normalised Difference Moisture Index (NDMI) and applying the Analytic Hierarchy Process (AHP) method. We developed fire severity models with the delta Normalised Burn Ratio (dNBR), the delta Normalised Difference Vegetation Index (dNDVI), and a wildfire susceptibility model using the AHP approach. The integration of these remote sensing tools and the GIS-based approach allowed, as the development of the proposal of a fire action plan and the establishment of a conceptual model, for wildfire management and prevention to support decision making in Vilcabamba parish. To accomplish this aim, we used geoprocessing tools such as the Geographic Information System (GIS) and GEE. We used the AHP method for the fire susceptibility model, selecting the most representative fire triggers in the study area. We chose this method because it allows us to include experts and community criteria for decision making and has been widely applied for fire susceptibility analysis. The versatility of the AHP method lies in integrating multiple layers of environmental information, meteorological conditions, and even local socio-economic conditions for forest management in hard-to-reach areas [26]. However, there are other methods, such as the Analytic Network Process (ANP), that are mainly applied for risk evaluations rather than susceptibility [27]. Finally, we validated the models with the field data of fires recorded in 2019 in the fire perimeter and statistical algorithms.

We selected the fire event of 3 September 2019, which occurred southwest of the parish, and it is considered the most representative background of fire dynamics in the region. By including the entire parish in this study, we can establish escape routes, considering the proximity to health centres, water bodies, fire stations, and fires that occurred in the sector in the last decade. Human activities provoked the fire of 3 September 2019, and it is recognised as the most representative in this region because it spread across 1837.64 ha and was extinguished in three days by firefighters [28]. Additionally, the Podocarpus National Park is located northeast of Vilcabamba parish, which has been declared a protected area of Ecuador according to the Ministry of Environmental, Water and Ecological Transition in Ecuador (MAE, Spanish acronym), a biodiversity hotspot in southern Ecuador with more than 560 bird species recorded [29].

This article is of great relevance for both environmental management and territorial planning because it provides a solid scientific basis for understanding the patterns and effects of forest fires, allowing the identification of the most vulnerable areas and the factors that contribute to their occurrence. Furthermore, implementing an action plan promotes effective preventive strategies, reduces the risks of future fires, and promotes the sustainable management of natural resources, especially in regions of high ecological value and vulnerability, such as Vilcabamba parish.

## 2. Study Area

In this case study, we analysed the severity of the wildfire that occurred on 3 September 2019, in the southwest part of Vilcabamba parish in the Andean region of Ecuador (Figure 1a) [30].

This parish belongs to Loja Province ( $79^{\circ}15'38.31''$  W and  $4^{\circ}13'8.38''$  S), which is located in the west part of the Catamayo-Chira basin (see Figure 1b). The Podocarpus National Park lies in the northeastern part of Vilcabamba parish, and, at the southwest area, there is the wildfire perimeter (Figure 1b). According to the National Secretary of Risks and Emergencies (SNGRE, Spanish acronym), 79 fires were recorded in Vilcabamba parish during the period 2011–2019 (pre-fire scene) [31].

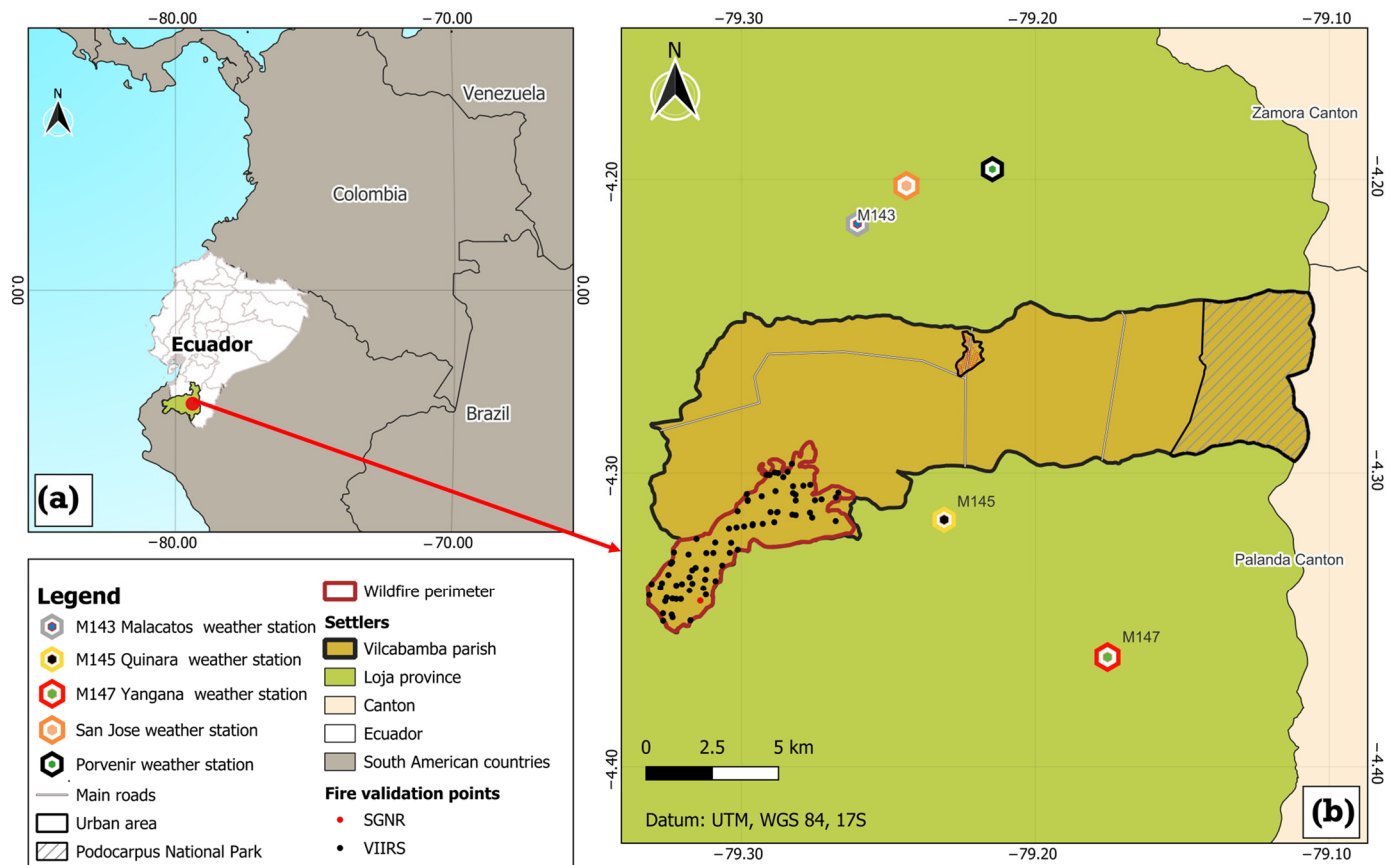


**Figure 1.** Location of the study zone: (a) Representation on a macro-scale (Ecuador); (b) Vilcabamba parish including the delineation of the wildfire perimeter analysed, weather stations, and the wildfires recorded in the year 2019 (pre-fire scene) by the SNGRE and VIIRS.

The Vilcabamba parish has a population of 5516 inhabitants [32] and an area of 15,932.61 ha. In this parish, there are outcrop cineritic volcanic rocks. An amount of 46.53% of the territory has a mountainous relief with slopes ranging from 70% to 100%. On the other hand, 56% of the parish has entisol soils, 36% inceptisol soils, and only 1.86% alfisol soils [33]. Vilcabamba parish has a temperate semiarid climate and distinct seasonal variations in altitudes from 1400 to 3750 m.a.s.l. [17]. According to Köppen climate classification [34], this sector has a mesothermal environment with a dry winter, considered a variety of the mesothermal humid climate type. This area experiences two main climate seasons (rainy and dry season). The rainy season typically occurs from October to May, while the dry season spans from June to September. According to the local weather stations (Malacatos (code M143), Quinara (code M145), Yangana (code M137), San Jose, and Porvenir stations), the average annual precipitation is around 875 mm, and the average yearly temperature is 19 °C. Finally, evapotranspiration is around 2268.1 mm/year.

The study area is characterised by its economy based mainly on agriculture and tourism. Agriculture is centred on cultivating coffee, sugar cane, fruits, vegetables, and products for local consumption and nearby markets. About 87% of the population is engaged in agriculture, forestry, hunting and fishing [33]. However, these agricultural



activities involve the removal of vegetation through the traditional use of fire, which, on numerous occasions, triggers forest fires [35]. During the period 22–25 August 2024, a fire was recorded in Quilanga canton, Loja province. In this fire, 738 ha of pine forest and grassland was affected, adding to the 8600 ha recorded in 2024 in Loja [36]. On the other hand, the tourism boom has encouraged the creation of inns, restaurants, and wellness centres, generating employment and, at the same time, contributing to changes in land use in the sector [37].

### 3. Materials and Methods

We conducted a bi-temporal analysis of Sentinel-2A imagery that might have some gaps in the collection due to the high levels of cloudiness typical in Andean regions. Therefore, we implemented a cloud-masking technique through the Google Earth Engine (GEE) environment to remove clouds in the satellite images. This study also allowed us to reduce interpretation errors in calculating spectral indices. This method is especially useful in Andean regions with high cloud cover, improving the usability of the image for terrain monitoring and analysis. We used GEE to process the selected remote sensing products.

The methodological approach includes four phases as shown in Figure 2: First, remote sensing methods (spectral indices for fire severity analysis) and geoprocessing tools (i.e., Geographic Information System (GIS) and GEE). Second, fire severity models using differentiated indices (dNDVI and dNBR) and a fire susceptibility model using the Analytic Hierarchy Process (AHP) method that considers variables such as slope angle, elevation, slope aspect, isohyets, isotherms, land use, distance to water bodies, and distance to roads. Third, the validation process for fire severity models and the fire susceptibility model. Fourth, the proposal of an action plan for fire management. This action plan includes the establishment of refuge areas, escape routes, and a conceptual model that evidences the fire triggers in the sector as a tool for decision-makers (governmental bodies and the community).

#### 3.1. Remote Sensing Tools for Fire Severity

##### 3.1.1. Remote Sensing Products

In this section, we used satellite imagery from Sentinel-2A [38], with the Multi-Spectral Instrument (MSI) that incorporates an atmospheric correction. This instrument has a radiometric resolution of 12 bits and 12 spectral bands. We developed a script code for the retrieval of a mosaic of the Sentinel-2A imagery using the cloud-based platform Google Earth Engine (GEE, Version: 2010, Google LLC, Mountain View, CA, USA) [39]. Subsequently, we applied the cloud-masking technique on the Sentinel-2A images selected in this study to remove areas with cloudiness greater than 30%. This method used the ‘maskClouds’ function of GEE, which refers to cloud probability values. We also set a cloudiness threshold to filter out pixels with high cloud probability, and those with a cloud probability below the selected threshold were retained.

The dates of the pre-fire and post-fire scenes were selected based on the following criteria: (i) dates before and after the fire on 3 September 2019, (ii) low cloud cover (less than 30%), and (iii) the availability of Sentinel-2A images during the dry season, which are the months with the highest occurrence of fires in the Vilcabamba parish (from June to September), as shown in Table 1.

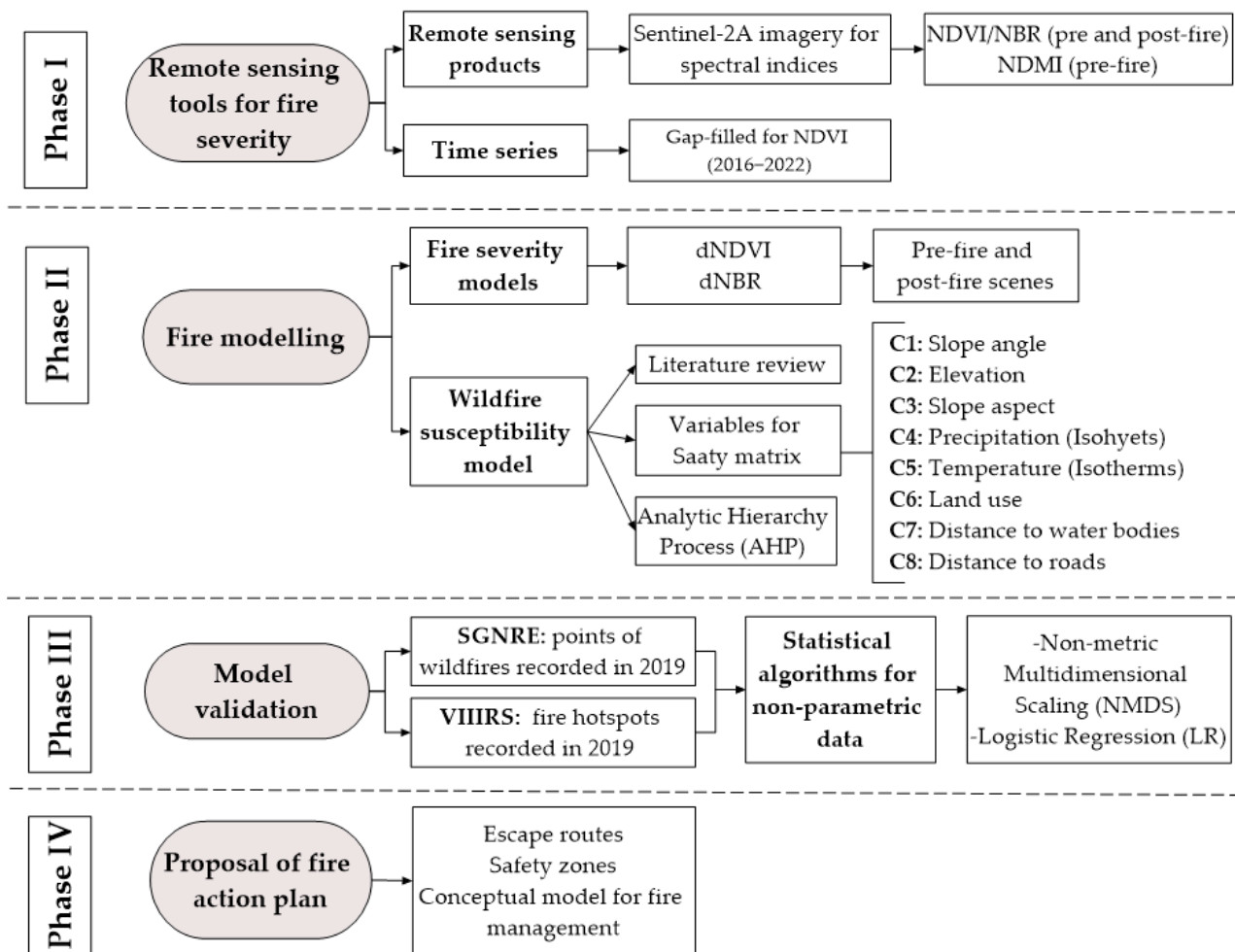


Figure 2. Methodological approach.

Table 1. Satellite data used for analysis in the study area.

Scene	Acquisition Date	Satellite	Cloudiness	Spatial Resolution	Source
Pre-fire	25 August 2019	Sentinel-2A	<30%	10 m	[40]
Fire-day	3 September 2019				
Post-fire	9 September 2019				
Post-fire	4 August 2021				

### 3.1.2. Spectral Indices

In this stage, we implemented a GEE script to calculate spectral indices for the assessment of fire severity. We calculated vegetation indices that use the normalised difference expressions derived from Sentinel-2A products. The selection of the most appropriate index was based on the following criteria: (1) clarify the presence or absence of burned areas within the Vilcabamba parish delimitation, comparing satellite data pre and post-fire, excluding water bodies, bare soil, and agricultural lands; (2) calculate vegetation indices from satellite data pre-fire (31 August 2019) and post-fire scenes (7 September 2019 and 5 August 2021). The spectral indices used in pre-fire and post-fire scenes are the Normalised Difference Vegetation Index (NDVI) and Normalised Burn Ratio (NBR). Finally, we calculated the Normalised Difference Moisture Index (NDMI) for the pre-fire scene. The equations and spectral bands used for these indices are shown in Table 2.

**Table 2.** Vegetation indices calculated for the case study.

Index	Equation	Spectral Bands	Source
NDVI	$NDVI = \frac{NIR - Red}{NIR + Red}$	Near-Infrared (NIR) Red	[41]
NBR	$NBR = \frac{NIR - SWIR2}{NIR + SWIR2}$	Near-Infrared (NIR) Short-Wave Infra-Red (SWIR) 2	[42]
NDMI	$NDMI = \frac{NIR - SWIR1}{NIR + SWIR1}$	Near-Infrared (NIR) Short-Wave Infra-Red (SWIR) 1	[43]

The NDVI indicates vegetation health and is used in environmental studies, monitoring crop conditions, and enhancing yield through precision farming practises [44]. The NDVI uses the Near-Infrared (NIR) band, which measures the amount of near-infrared light reflected by vegetation, and the Red band, which measures the amount of red light reflected. Otherwise, the NBR maps fire severity from high severity to unburned areas and tracks vegetation changes in post-fire environments, providing a quantitative measure of the severity and extent of fire damage [45]. This analysis enhances the contrast between burned and unburned areas, reducing the impact of topography and soil moisture [42]. Finally, the NDMI is a proxy for vegetation stress that measures the levels of moisture in vegetation and is useful for monitoring drought conditions, crop health, and assessing the overall moisture status of vegetation [43].

The use of vegetation indices in remote sensing and environmental monitoring is valuable. Still, it has several limitations, such as its sensitivity to atmospheric conditions (e.g., clouds, aerosols, and water vapour), which can distort reflectance values and lead to inaccurate assessments [46]. In addition, these indices usually affect measurements in mixed pixels that are less accurate when non-plant elements such as soil or water are present [47]. Therefore, vegetation indices should be complemented by other methods, such as the cloud-gap-filled (CGF) method, that will allow a comprehensive understanding of vegetation health and dynamics [22]. For instance, the CGF method has been applied in India for the removal of clouds in the calculation of the Normalised Difference Snow Index [48]. In this study, we applied the CGF method through the GEE random forest algorithm. In addition, we analysed the resulting values of vegetation indices with GIS information layers of water bodies, land use and urban areas to remove these interpretation limitations in Andean regions.

We implemented the cloud-gap-filled method as a masking technique to enhance the accuracy of the NDVI time series [49]. This method also reduces the effects of cloudiness with the application of filters to remove clouds and shadows. Subsequently, we generated a continuous NDVI time series from 2016 to 2022 in a way that we can monitor vegetation dynamics in pre-fire and post-fire scenes as shown in Figure S1. This technique fills the missing data using the best estimation neighbouring points from earlier and later observations through interpolation. The gaps were filled with the joint function from GEE, applied to imagery mosaics. This technique is primarily applied in vegetation indices, climatological data, high-resolution multispectral images, and time series [50]. Finally, the GEE code used in this study is as follows: <https://code.earthengine.google.com/667193383cfacacefdd0bd1486f3accf> [51].

### 3.2. Fire Modelling

#### 3.2.1. Fire Severity Models

In this section, we used the differentiated indices, delta Normalised Difference Vegetation (dNDVI), and delta Normalised Burn Ratio (dNBR) using the pre-fire scene (2019) and post-fire scene (2021), as shown in Equations (1) and (2), respectively. We implemented

these fire severity models to assess the severity of the event in Vilcabamba parish and the amount of burned areas after two years of the fire event of 3 September 2019.

$$dNDVI = \text{pre-fire NDVI} - \text{post-fire NDVI} \quad (1)$$

$$dNBR = \text{pre-fire NBR} - \text{post-fire NBR} \quad (2)$$

### 3.2.2. Fire Susceptibility Model Using AHP Multi-Criteria Method

In this section, we applied the GIS-based multi-criteria analysis that uses the Analytic Hierarchy Process (AHP) method for the generation of a wildfire susceptibility model in Vilcabamba parish. Thomas L. Saaty developed the AHP method in the 1970s [52], a multi-criteria decision-making tool for dealing with complex problems. The AHP is considered one of the most effective models for risk assessment [53] and has been widely used in Geographic Information Systems (GISs). This model benefits spatial analysis, although it does not focus on problem conceptualisation. It uses geographic data and map algebra to identify areas susceptible to wildfire, assigning a weight to each criterion according to its relevance based on available experience, information and skills [54]. This method uses geographic information to ascertain the probability of wildfires, which requires a comprehensive database for storing all the variables. Therefore, we use QGIS (version 3.16.0, ESRI, Boston, MA, USA) and ArcGIS Pro (version 3.1, QGIS Development Team, Redlands, CA, USA) software for spatial analysis. Decision theory represents a multidisciplinary theory that uses different methods (e.g., the Analytic Hierarchy Process (AHP) method) to guarantee the quality of a decision in management processes. The AHP guarantees quality because it has a robust mathematical base and is to be used in evaluating and selecting the best alternatives to explain a phenomenon [55], in this case, triggers for fire severity. There are other methods such as the Decision Matrix Method (DMM) [56] and the Forced Decision Matrix Method (FDMM) [57] that effectively assess the selection of factors for decision-making approaches. However, the AHP method was selected due to the simplicity of sharing with community and receiving their opinions in the best selection of triggers for fire severity in Vilcabamba parish, considering climate and socio-ecological conditions.

Predicting forest fires is challenging because these events could have natural or anthropic origins. Therefore, we selected eight variables (C1 to C8) that better represent fire susceptibility in Vilcabamba parish as a guideline for decision-makers. The variables are the most significant triggers in the study area according to the literature review and analysis of the baseline data in the study area.

- Distance to roads (C8): The fire analysed was provoked by human activities. Therefore, knowing the distance to roads is a reference to the proximity to urban zones that are the main triggers for fire-starting events in Vilcabamba parish, considering that humans generate 99% of forest fires in Ecuador [58].
- Distance to water bodies (C7): This includes superficial water sources such as rivers, streams, lakes, and lagoons that can provide water in case of fire events. The AHP method uses the weighted overlay tool that incorporates surface restrictions based on this variable, providing clues for understanding wildfire events [59]. We determined these variables using the Euclidean distance technique that calculates the distance to every single point of the geographic space.
- Land use (C6): This is crucial in the probability of forest fires in this sector because humans generate forest fires through poor farming practises such as burning grasslands that change the land use dynamics and affect fire intensity. For this variable, we used data from the geoportal of the Ministry of Environmental, Water and Ecological Transition in Ecuador (MAE, Spanish acronym) from 2018 for pre-fire and 2022 for post-fire scenes [60].
- Temperature (C5), and precipitation (C4): These create the necessary conditions for fires to burn with a certain magnitude. For precipitation (isohyets) and temperature (isotherms), we used data from five meteorological stations (Malacatos, Quinara,

Yangana, Porvenir, and San Jose stations), located 15 km from Vilcabamba parish (Figure 1b). Yanacocha and San Jose stations are monitored by the National University of Loja (UNL, Spanish acronym) from 2016 to the present [61] and measure variables such as the following: temperature, precipitation, wind speed, wind direction, and relative humidity on a daily scale with a frequency of 15 min. Meanwhile, Malacatos, Quinara, and Yangana stations are monitored by the National Institute of Meteorology and Hydrology (INAHMI, Spanish acronym) [62].

- Slope angle (C1): This parameter is vital because it influences the spread of fire, with steeper slopes allowing fire to move faster uphill, as gravity helps spread flames [63]. It also affects wind patterns and fuel availability, as steeper terrains can concentrate heat and increase fire intensity.
- Elevation (C2), and slope aspect (C3): These variables are essential but not determinants for starting a forest fire in Vilcabamba parish. For these variables, we used the Digital Elevation Model (DEM) of the Military Geographical Institute (IGM, Spanish acronym) [64]. For the calculation of the slope angle and aspect, we use the GIS-based geodesic method and the QGIS software. This method is also known as Earth Centred, Earth Fixed (ECEF), as it considers the earth as an ellipsoid and shapes the slope in 3D through Cartesian coordinates [65].

Table 3 includes the source for the eight variables selected, their spatial resolutions, and the importance of each variable using a scale of importance from 1 to 4, where 1 = null susceptibility, 2–3 = Low–Moderate, and 4 = High. For the weights of the variables, the AHP method assigns them according to their relative importance. These weights were adapted from the multi-criteria matrix proposed by Saaty [52], considering the scientific literature from studies with similar climatic conditions to Vilcabamba parish. For example, Ibarra (Ecuador) [65] and Bolivia [66] have an intrinsic connection in the composition of the different altitudinal floors, which allows us to rank the variables with greater precision.

**Table 3.** Variables for the wildfire susceptibility analysis for Vilcabamba parish.

Variables	Resolution (m)	Period	Preparation Method	Weight	Score	Variable Importance	Source
C1: Slope angle (%)	30 × 30	2020	geodesic (ECEF method)	15%	15 30 45 60	1 2 3 4	[64]
C2: Elevation (m.a.s.l.)	30 × 30	2020	Classification	5%	1400–1500 1500–2250 2250–3000 3000–3750	1 2 3 4	[64]
C3: Slope aspect	30 × 30	2020	geodesic (ECEF method)	4%	Flat South West East North	1 2 4 3 1	[64]
C4: Mean annual precipitation (mm)	30 × 30	2016–2023	IDW Interpolation	8%	500–750 750–1000 1000–1250 1250–1500	1 2 3 4	[61]
C5: Mean annual temperature (°C)	30 × 30	2016–2023	IDW Interpolation	12%	8–10 12–14 16–18 20–22	1 2 3 4	[61]
C6: Land use	1:250,000	2018–2022	Clipped from MAE geoportal	17%	Forest Water bodies Other lands Agriculture lands Shrub and herbaceous vegetation Urban zone	4 1 2 3 4 1	[60]



Table 3. Cont.

Variables	Resolution (m)	Period	Preparation Method	Weight	Score	Variable Importance	Source
C7: Distance to water bodies (m)	30 × 30	2020	Euclidean distance	18%	140 280 420 560	4 3 2 1	[67]
C8: Distance to roads (m)	30 × 30	2020	Euclidean distance	21%	300 600 900 1200	4 3 2 1	

Note: ECEF: Earth Centred, Earth Fixed; IDW: Inverse Distance Weighting; MAE: Ministry of Environmental, Water and Ecological Transition in Ecuador, Water and Ecological Transition in Ecuador; variable importance: 1 = null susceptibility, 2–3 = Low–Moderate, and 4 = High.

We applied the GIS-based tool named “Weighted overlay” that performs the algebra of maps and weights for each predictor selected (C1 to C8) based on the multi-criteria AHP method (Figure 3).

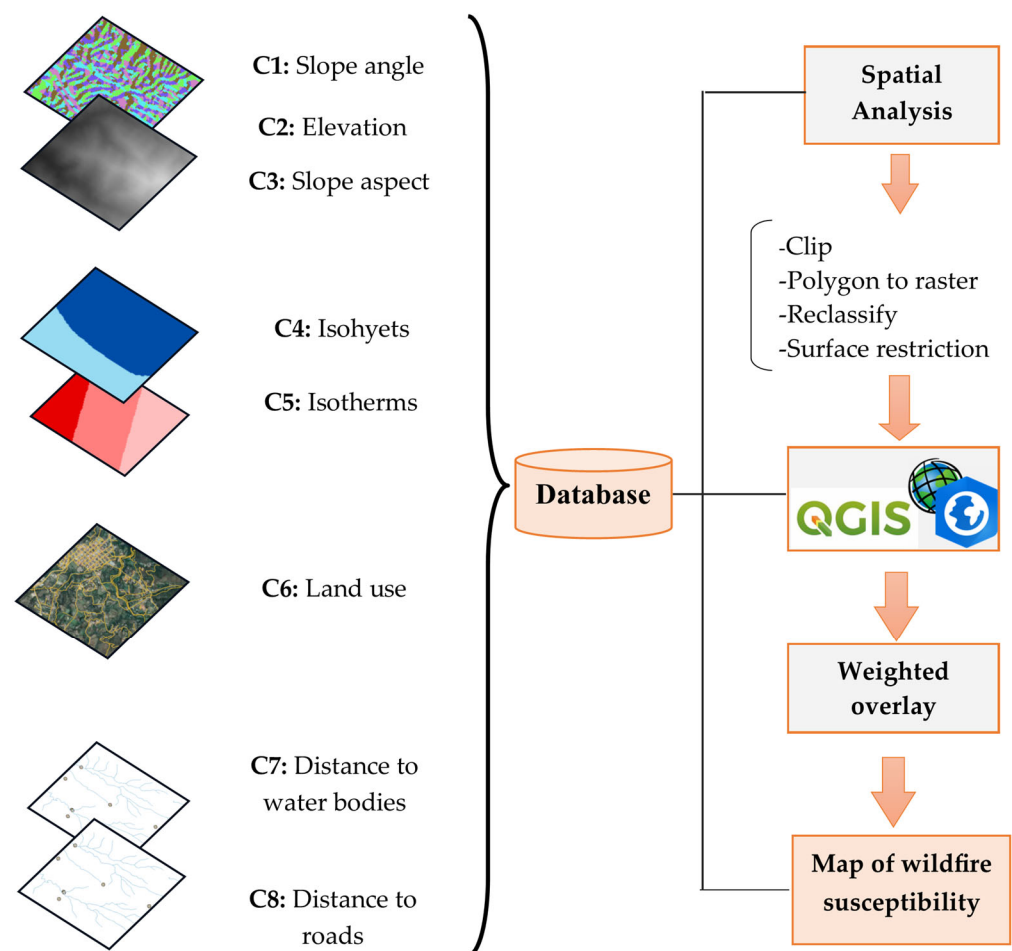


Figure 3. Framework of the wildfire susceptibility analysis using the AHP method.

Equations (3) and (4) allow the calculation of the Eigenvector ( $V_p$ ) and the coefficient of the weights ( $C_p$ ), where “W” represents the weights, and “k” is the number of variables. Subsequently, to calculate the coherence coefficient (CR), we use Equation (5) that validates the calculated weighted weights and Equation (6) for the coefficient of the weights for each variable (CI). Finally, we calculated the random consistency index (Rci), which varies according to the number of elements compared, where “ $\lambda_{max}$ ” represents the

maximum eigenvalue of the matrix, and “n” corresponds to the number of variables used (Equation (7)).

$$V_p = \sqrt[k]{W_1 * W_2 * W_3 * W_k} \quad (3)$$

$$C_p = \frac{V_p}{V_{p_1} + \dots + V_{p_k}} \quad (4)$$

$$CR = \frac{CI}{Rci} \quad (5)$$

$$CI = \frac{\lambda_{\max} - n}{(n - 1)} \quad (6)$$

$$Rci = \frac{1.98 - (n - 2)}{n} \quad (7)$$

Table 4 shows the level of importance for the variables considered with the AHP criteria. We used paired comparisons and an adapted scale outlined in another Andean region [65].

**Table 4.** Scale for pairwise comparisons.

Score	Definition
9	Extreme importance
6; 7; 8	Very strong importance
4; 5	Strong importance
2; 3	Moderate importance
1	Equal importance of one over the other variable

Table 5 shows the assessment of the relative importance of the wildfire susceptibility variables by comparing two factors/variables simultaneously, as verified with a literature review [65,66,68]. The pairwise comparison matrix places the factors in rows and columns with a principal diagonal value of 1 and the relative weight of the comparison in each cell.

**Table 5.** Pairwise comparison matrix applied to variables in Vilcabamba parish.

Variables	C1	C2	C3	C4	C5	C6	C7	C8	Vp	Ci	λi
C1	1.00	5.00	7.00	7.00	1/8	7.00	1/4	1/5	1.35	0.15	2.71
C2	1/5	1.00	2.00	1/2	1.00	1/8	1/6	1.00	0.50	0.05	1.33
C3	1/7	1/2	1.00	1.00	1/5	1/8	1/2	1/6	0.33	0.04	0.00
C4	1/7	2.00	1.00	1.00	2.00	1.00	1/4	1.00	0.78	0.08	0.01
C5	8.00	1.00	5.00	1/2	1.00	1/4	1/2	1.00	1.12	0.12	1.37
C6	1/7	8.00	8.00	1.00	4.00	1.00	1.00	1.00	1.57	0.17	1.95
C7	4.00	6.00	2.00	4.00	2.00	1.00	1.00	1/6	1.68	0.18	1.76
C8	5.00	1.00	6.00	1.00	1.00	1.00	6.00	1.00	1.91	0.21	1.14
Σ	18.63	24.50	32.00	16.00	11.33	11.50	9.67	5.53	9.25	1.00	10.27

Note: C1: slope angle, C2: elevation, C3: slope aspect, C4: precipitation, C5: temperature, C6: land cover, C7: distance to water bodies, C8: distance to roads, Vp: characteristic vector, Ci: coefficient of the weights for each variable, and λi: maximum eigenvalue of the matrix.

WF in Equation (8) represents the fire susceptibility analysis by applying the multi-criteria AHP method through the weighted overlay tool, which performs the map algebra and assigns weights to each of the eight predictors (C1 to C8).

$$WF = (0.06 \times C1) + (0.09 \times C2) + (0.10 \times C3) + (0.15 \times C4) + (0.13 \times C5) + (0.14 \times C6) + (0.08 \times C7) + (0.25 \times C8) \quad (8)$$

The calculated CI was 0.12, and, then, it was divided by the Rci (1.48) to obtain a value of CR = 0.027. The CR obtained is consistent because it is less than 0.10, demonstrating that the model is good. The fire susceptibility model was based on eight variables obtained from official mapping sources, categorising fire susceptibility as null, Low–Moderate, and High.

### 3.3. Model Validation

We validated the fire severity models (dNDVI and dNBR) and the fire susceptibility model with 78 points of registered fires in the year 2019. This information was distributed as follows: 77 points of fire hotspots were collected from the Active Fire Product of Suomi NPP Visible Infrared Imaging Radiometer Suite (VIIRS) and 1 point from the SNGRE. These data have a binary value of 0 and 1, where 0 represents the absence of fires, and 1 the presence of these fire events in the pre-fire scene (year 2019). In Table 6, we present the exploratory analysis of the data before selecting the model validation algorithms, verifying the non-normality of the data as the kurtosis exceeds the range between  $-3$  and  $+3$ .

**Table 6.** Exploratory analysis of the validation data.

Parameters	dNBR	dNDVI	AHP Model	Normality Ranges
Skewness	0.10	1.19	−3.55	[−3, +3]
Kurtosis	5.18	5.57	8.66	[−3, +3]

Once the non-normality of the data was determined, we used the software RStudio (Version 4.2.3, Posit PBC, Boston, MA, USA) to calculate two statistical algorithms (Logistic Regression (LR) and Non-metric Multidimensional Scaling (NMDS)). For the Logistic Regression [69], we used the packages “ROCR”, “ggplot2” and “pROC”. For the Non-metric Multidimensional Scaling [70], we implemented the “vegan”, “ggplot2” and “viridis” RStudio packages and the “metaMDS” function [71].

The LR model predicts a “probability value” through a linear combination of the given features included in a logistic function that uses a binary value of 0 and 1, where ‘0’ corresponds to the absence of fire and ‘1’ for the presence of fire. On the other hand, the NMDS algorithm assesses the similarity between samples (78 fire points recorded in the year 2019 for pre-fire scene). This method is analogous to Principal Component Analysis (PCA) in that it identifies groups based on a suite of variables. However, the NMDS does not have the limitation of multivariate normality and multivariate homoscedasticity assumptions (i.e., it assumes that different samples have the same variance, even if they come from different populations) [72].

### 3.4. Proposal of Action Plan for Wildfire Management

In this phase, we drew up a proposal for an action plan for fire management in Vilcabamba parish by considering factors that included the proximity to settlers, river networks, the road infrastructure, the location of health centres, historical fire records, and land use for the identification of regions with high probability to burn. For the historical fire records, we used the on-site fire points in the period 2011–2019 (pre-fire conditions), obtained from the SNGRE. Additionally, we used VIIRS fire probability points for the period 2012–2019. We established escape routes, safety zones, and a conceptual model for wildfire management in the study area. We used Dijkstra’s shortest path algorithm (Road Graph plugin) to identify refuge zones within the QGIS framework. This plugin improves the decision-making processes in the event of an unanticipated wildfire by synthesising geospatial data, including road networks, topographic attributes, and potential obstructions, combining advanced geospatial insights and computational algorithms [73]. This analysis

calculates the distance between fire stations and selected fire probability points, which are vectors strategically located according to previous analyses such as the zones with high fire susceptibility obtained from the AHP approach (Section 3.2) and the fire severity levels from the differentiated indices dNDVI/dNBR (Section 3.3). Finally, we selected the shortest escape route given the road network options in the study area and considering the fire susceptibility map.

Figure 4 summarises a conceptual model for fire management in Vilcabamba parish. This model considers the remote sensing tools applied, the wildfire drivers identified within the AHP approach, and the action plan's primary results, such as the escape routes and refuge zones. These results are vital for the effective containment and control of fire outbreaks, thereby minimising potential damage to settlements and ensuring the safety and well-being of the inhabitants in the parish.

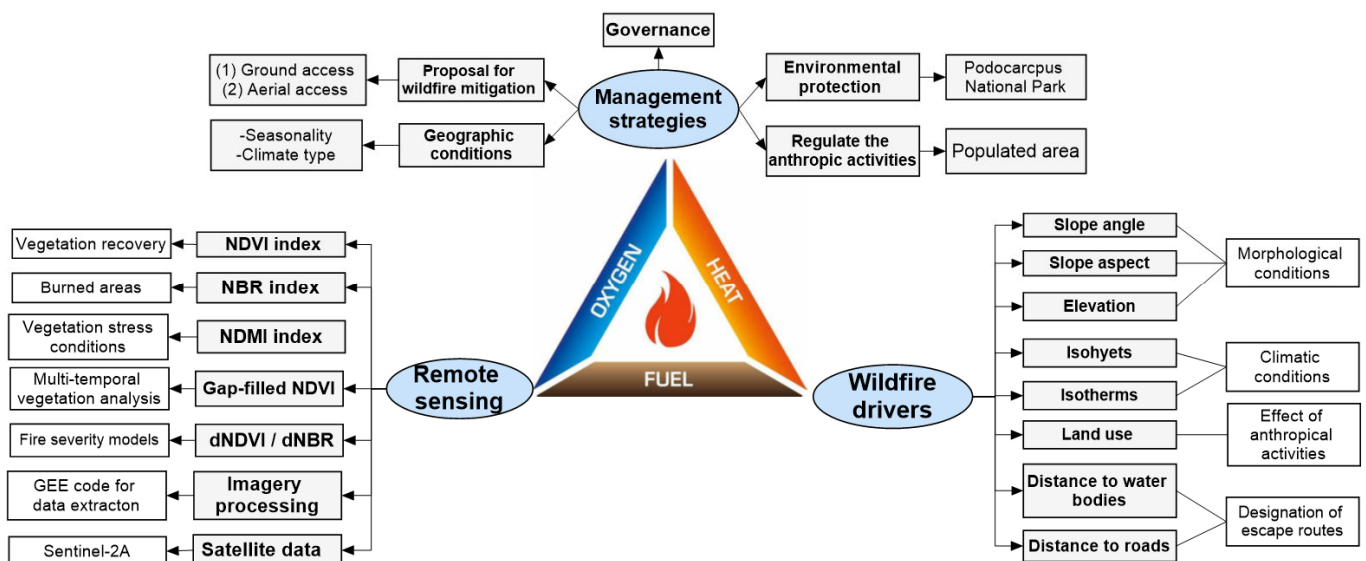


Figure 4. A conceptual model for wildfire management in Vilcabamba parish.

## 4. Results

### 4.1. Assessment of Wildfire Severity with Spectral Indices

#### 4.1.1. Burned Areas Using NBR Index

The NBR index uses six categories adapted according to studies with geographical similarities [25,60]. In the pre-fire scene (Figure 5a) of the fire perimeter, it was identified that 52.58% corresponded to unburned areas and 7.33% to areas with high vegetation regeneration. In the post-fire analysis performed days after the event (Figure 5b), it was observed that 10.98% corresponded to burned areas with moderate–high severity and 64.45% to burned areas with moderate–low severity. In contrast, the NBR index calculated two years after the event (Figure 5c) showed that 0.01% corresponded to burned areas with moderate–high severity, while 83.82% were classified as areas with low vegetation regeneration and 12.41% as areas with high vegetation regeneration.

The NBR results demonstrate a clear contrast between pre- and post-fire conditions. In the pre-fire image, low levels of severity are evident, indicating that the vegetation had not been significantly affected and that the ecosystem was in a relatively stable condition. On the other hand, in the image captured after the fire, high recovery rates are observed. Over time, the vegetation has regenerated noticeably, showing signs of ecological resilience. This change reflects the ability of the ecosystem to recover after a significant disturbance. However, the rate and magnitude of recovery may depend on several factors, such as soil characteristics, the availability of water resources, and the absence of further disturbance.

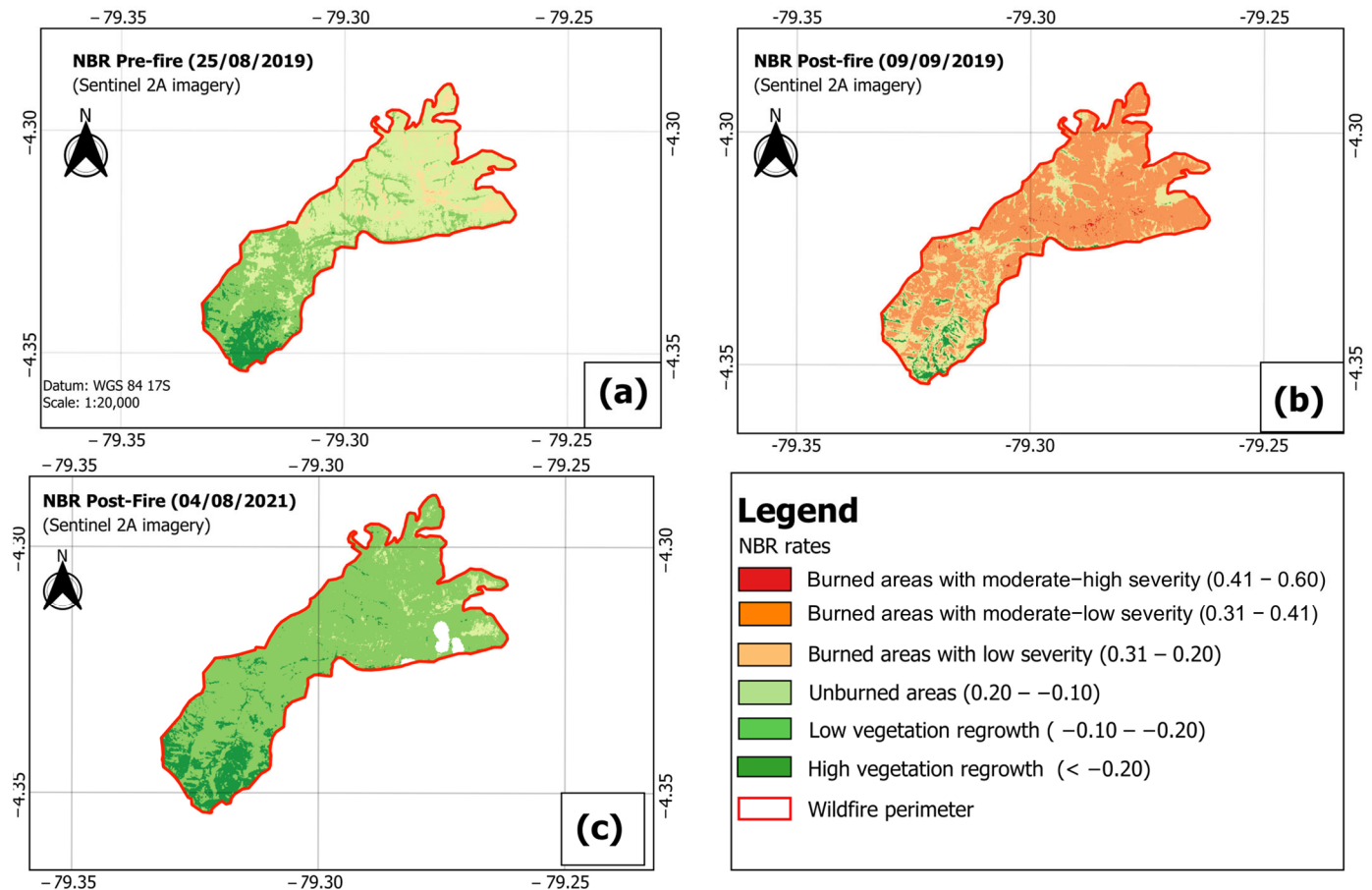


**Figure 5.** NBR index in fire perimeter with Sentinel-2A imagery: (a) Pre-fire scene (9 September 2019); (b) Post-fire scene (9 September 2019); and (c) Post-fire scene (4 August 2021).

The application of the NBR index in the study area reveals the ecological resilience of the post-fire ecosystem, highlighting a significant transition in vegetation conditions. In the pre-fire scene, the low severity observed indicates relative stability. At the same time, the post-fire scenes evidenced a progressive increase in areas of vegetation regeneration, especially two years after the event. This finding underlines the resilience of the ecosystem, although the predominance of low regeneration areas (83.82%) highlights the need for management strategies to favour a more uniform and effective recovery.

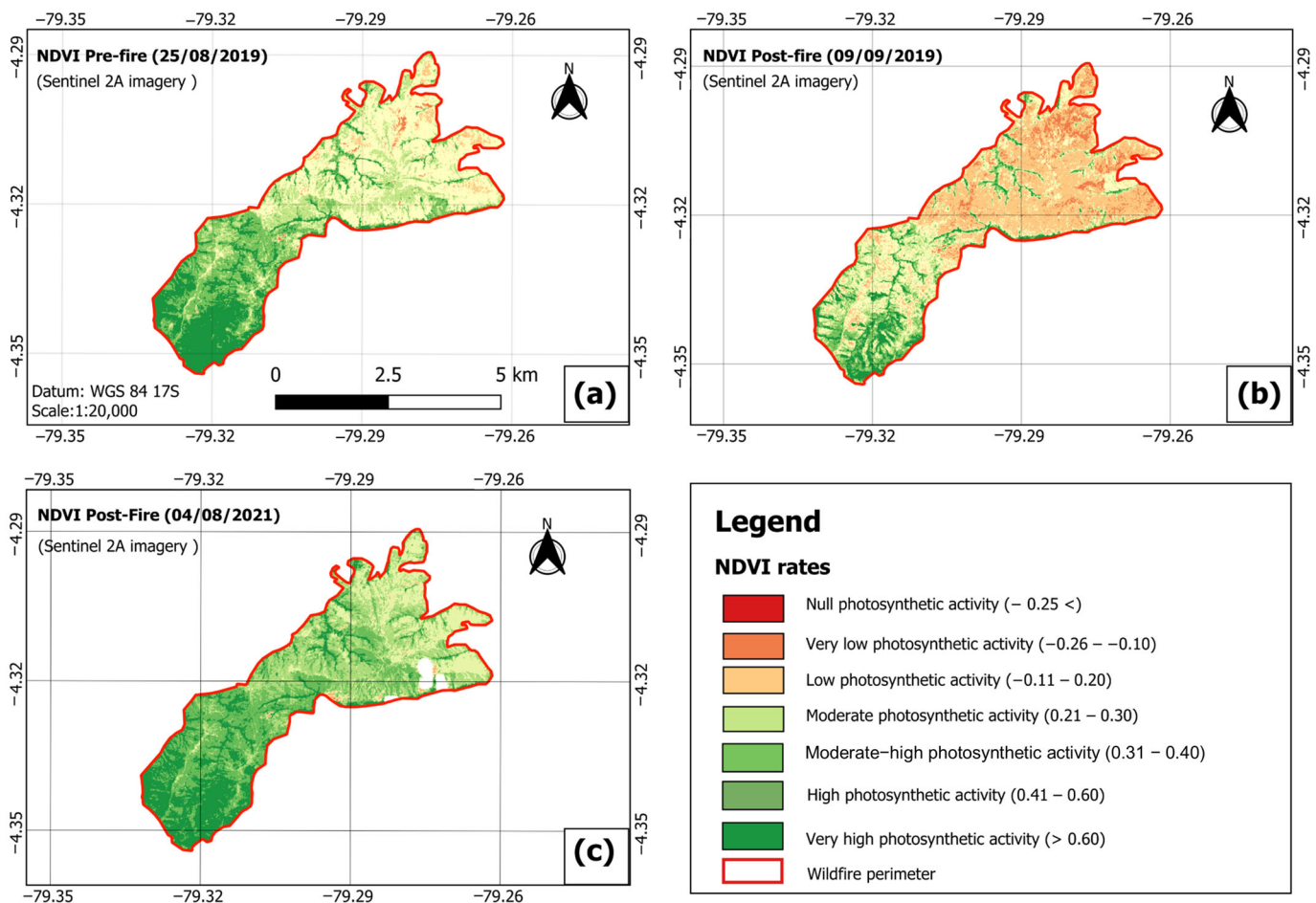
#### 4.1.2. Vegetation Recovery Using NDVI Analysis

In the pre-fire scene (2019, Figure 6a), 21.45% of the area shows high photosynthetic activity. On the other hand, in the post-fire scene captured a few days after the event (Figure 6b), there was a notable decrease of 45.83% in high photosynthetic productivity in the parish of Vilcabamba. Finally, in the post-fire scene 2021 (Figure 6c), 30.50% of low photosynthetic activity and 11.57% of high photosynthetic activity were recorded, confirming a moderate recovery two years after the fire analysed in this study.

NDVI analysis reveals a drastic decrease in high photosynthetic activity after the fire, followed by a moderate recovery two years later. This pattern underlines the significant impact of fire on vegetation productivity and the ability of the ecosystem to regenerate over time. However, the persistence of areas with low photosynthetic activity highlights the influence of limiting factors, such as local edaphic and climatic characteristics. This finding emphasises the importance of implementing specific management and restoration strategies focused on the most affected areas to accelerate ecological recovery and improve the landscape's resilience to future disturbances. In addition, the continuous monitoring



of photosynthetic activity can serve as a critical indicator to assess the success of such strategies and adapt conservation policies.



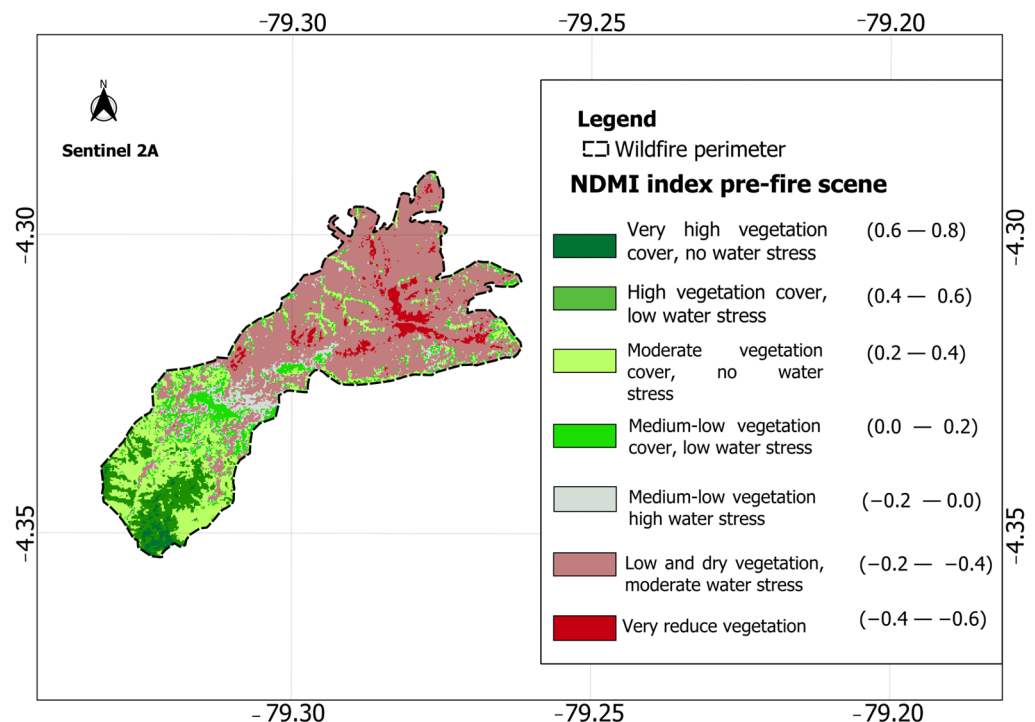
**Figure 6.** NDVI results of fire perimeter: (a) Pre-fire scene (25 August 2019); (b) Post-fire scene (9 September 2019); and (c) Post-fire scene (4 August 2021).

Figure S2 presents a compelling demonstration of the long-term NDVI calculation in Vilcabamba parish using the cloud-gap-filled method. This technique was vital to recognise the tangible impact of the forest fire on the study area by filling in the gaps displayed in the original time series during January 2016, July 2017, and November 2020 (Figure S1). The impact of wildfire is borne from the reduction in the NDVI to 0.3 in October 2019, one month after the fire analysed in this study, which indicates low vegetation productivity (Figure 5). Remarkably, the NDVI records a sharp contrast during May 2022 (three years after the fire day) with an NDVI value of 0.545 (high photosynthetic activity) due to the onset of the rainy season. These results clearly diagnose the vegetation dynamics and the constant oscillations in the NDVI caused by dry and rainy seasons in the study area. Therefore, it is an approach that future studies can replicate in regions with similar geographical and climate conditions.

#### 4.1.3. Vegetation Stress Conditions Using NDMI

Figure 7 shows the NDMI calculated in the fire perimeter with Sentinel-2A imagery in the pre-fire scene (dry season) because most fires are generated from June to September in this region. The NDMI is a pillar for fire severity analysis because it presents the moisture and water stress conditions of the fire perimeter zone, giving us evident patterns of the state of the vegetation in the pre-fire scene. The NDMI ranges were adapted based on a literature review in Andean areas with conditions similar to those of the study area, such

as the Colombian Andes [74]. NDMI values from  $-0.2$  to  $-0.4$  correspond to low and dry vegetation and represent 52.62% of the fire perimeter. Meanwhile, in the southwest zone of the wildfire perimeter, 8.27% has high vegetation cover with low water stress.



**Figure 7.** NDMI results of Vilcabamba parish in pre-fire scene.

This analysis provides evidence that the environmental characteristics and conditions before the wildfire occurred were conducive for an event of this magnitude. Prevailing factors such as dry biomass accumulation, high temperatures, low relative humidity, and terrain topography created an environment highly susceptible to the development and spread of a large-scale fire. Under these circumstances, any human activity or anthropogenic interaction, whether accidental or intentional, would have the potential to act as a trigger, generating a fire that would quickly reach considerable dimensions and be challenging to control.

#### 4.2. Fire Severity Models Using Differentiated Indices

The dNDVI and dNBR models computed with Sentinel-2A images consider observations of pre-fire (2019) and post-fire (2021) scenes within six categories of fire severity. We selected the severity categories with the support of a literature review [75,76]. Figure 7 shows that the high severity values from the dNDVI and dNBR were very similar despite these indices using different spectral bands and fire severity categories for their calculation. These models allow the assessment of damage severity and vegetation regeneration between the pre-fire (2019) and post-fire (2021) periods. In Figure 8a, unburned areas represent 10.11% of the total fire perimeter extent, while areas of very low severity represent 85.77%. This analysis suggests that most affected areas show low severity, although some areas show high and very high severity, indicating a significant impact of the fire in certain parts. In Figure 8b, the dNBR index highlights vegetation recovery in the post-fire phase. Areas with high and low enhanced regeneration are shown in shades of green, indicating positive progress in recovery, while affected areas with low to high severity are represented in colours ranging from yellow to red. The validation points in both models corroborate the presence of areas of enhanced recovery in the north, although recovery is heterogeneous around the fire perimeter.

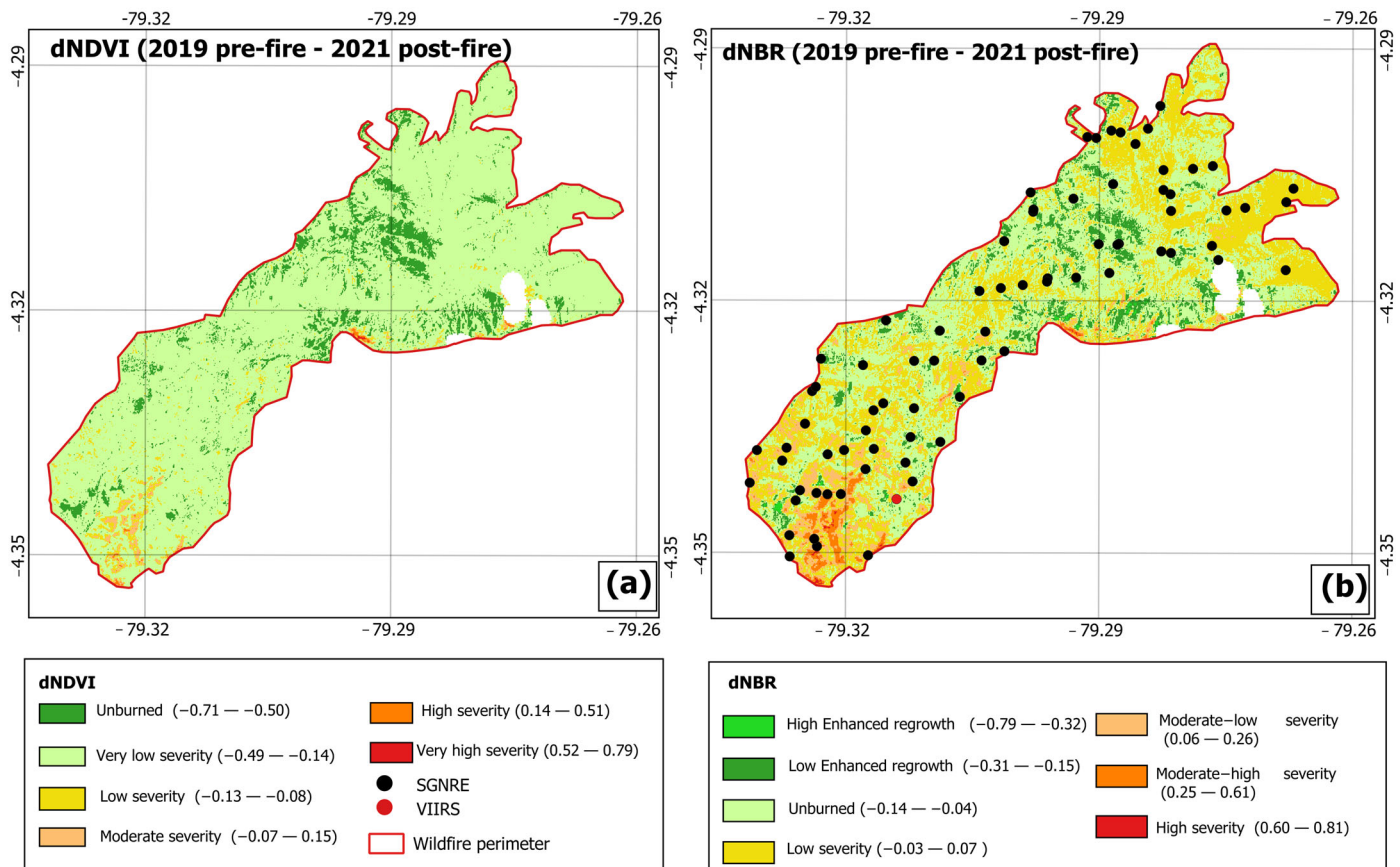


**Figure 8.** Wildfire severity models with Sentinel-2A imagery. (a) dNDVI and (b) dNBR.

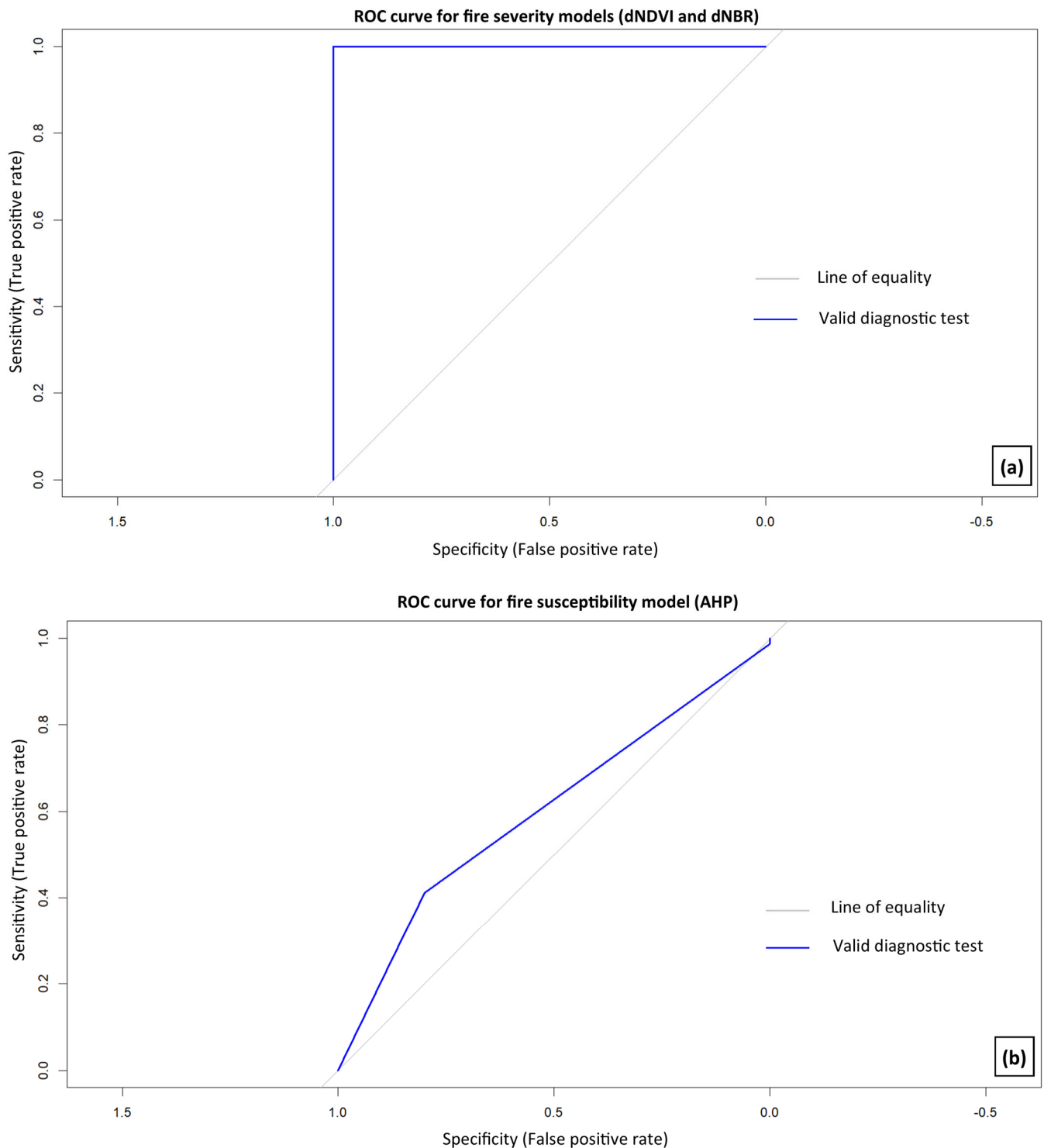
The combined analysis of the dNDVI and dNBR allows for a comprehensive assessment of the fire's initial impact and vegetation's recovery over time. The results show that, although most affected areas have low severity, the high and very high severity areas reflect significant impacts on specific parts of the fire perimeter. As evidenced by the dNBR, vegetation regeneration shows positive progress, especially in northern regions, although recovery is uneven across the landscape. These findings underline the importance of prioritising targeted restoration strategies in the most affected areas.

Table 7 presents the validation using the Logistic Regression (LR) and the Non-metric Multidimensional Scaling (NMDS) algorithms. This analysis shows that the fire severity models (dNBR and dNDVI) are more statistically significant than the fire susceptibility model in explaining the fire phenomenon in Vilcabamba parish. The Logistic Regression model used the Area Under Curve (AUC) as an accuracy representation of the LR model, thereby presenting the highest accuracy in both the dNBR and the dNDVI with an AUC of 1.0. For the AHP model, the AUC has a value of 0.6 that is acceptable but with lower accuracy than the fire severity models (Figure 9).

**Table 7.** Validation of fire severity models using two statistical algorithms.

Algorithm 1	AUC dNBR	AUC dNDVI	AUC AHP	AIC
LR	1.00	1.00	0.60	6
Algorithm 2	RMSE	Max Residual	Stress	Model
NMDS	0.006	0.031	0.032	severity models
NMDS	0.031	0.093	0.094	AHP model

Note: LR: Logistic Regression; NMDS: Non-metric Multidimensional Scaling; AUC: Area Under Curve; AIC: Akaike information criterion; RMSE: Root Mean Square Error; and Stress: number of dimensions.



**Figure 9.** Area Under Curve for the Logistic Regression model: (a) the AUC for the fire severity models and (b) the AUC for the fire susceptibility model.

The Non-metric Multidimensional Scaling model presented higher accuracy than the LR model, which is verified with the Root Mean Square Error (RMSE), as the lower the RMSE, the better the fit of the model of a dataset [77]. The NDMS has an RMSE value near zero (0.006) for the severity models and the RMSE = 0.94 for the AHP model. Additionally, the stress value that represents the specified number of dimensions explains how well points fit the NMDS model [78]. The fire severity models have a stress value of 0.032 and 0.094 for the AHP model, which likely indicates a good fit model.

The Receiver Operating Characteristic (ROC) is a graphical representation used to evaluate the performance of binary classification models, showing the relationship between the True Positive Rate (TPR) (Equation (9)) and the False Positive Rate (FPR) (Equation (10)) across different thresholds.

$$\text{Sensitivity} = \text{TP} / (\text{TP} + \text{FN}) \quad (9)$$

where

TP = true positives;

FN = false negatives.

$$\text{Specificity} = \text{TN} / (\text{FP} + \text{TN}) \quad (10)$$

where

TN = true negatives;

FP = false positives.

The ROC curve in Figure 9a plots the relationship between these two metrics as the classification threshold is adjusted. An ascending curve is observed, indicating that, as sensitivity increases, the false positive rate also increases, which is typical of classification models that tend to classify more instances as positive. The shape of the curve and its proximity to the specificity axis suggest that the model is close to optimal performance as it approaches the upper left corner, indicating high sensitivity and specificity. Figure 9b shows a behaviour where the curve follows an almost vertical path towards the top of the sensitivity axis and then moves horizontally along the specificity axis. This pattern suggests that the model performs well, with a high sensitivity (close to 1) at specific specificity values. The curve indicates that the model has a low false positive rate (high specificity) for the classification thresholds used. The shape of the curve also suggests that the model is robust enough to provide a good balance between sensitivity and specificity, which could lead to reconsidering the threshold or classification technique used.

#### 4.3. Analysis of Variables for Wildfire Susceptibility

For the AHP analysis, we considered eight variables. First, Figure 10a (C1) shows that 60% of the slopes are concentrated in the northwest and west directions, 20% south, and the remaining 20% (east and west) in the fire perimeter. Second, Figure 10b (C2) shows the changes in elevation in the study area that range from 1400 to 3750 m.a.s.l. The aspect map (C3, Figure 10c) shows that 31% of all the hillside orientations are in the north and northwest zones of Vilcabamba parish, implying that the orientation of the slopes has a low influence because they receive fewer daylight hours per day. The isohyets (C4 in Figure 10d) show annual precipitation from 500 mm to 1500 mm, and the isotherms (C5 in Figure 10e) show annual temperatures from 8 °C to 22 °C. Figure 10f–g shows the changes in land use (C6) in the Vilcabamba parish, considering the pre-fire (2018) and post-fire (2022) scenes. Figure 10h represents the distance to water bodies (rivers and streams), considered for ground-based fire monitoring because they are closer to the firefighters in the event of a wildfire. Finally, Figure 10i includes the distance to roads that range from 0 to 8 km.

The analysis of land use shows a reduction in shrub and herbaceous vegetation areas, from 64.15% in pre-fire to 61.62% for the post-fire scene (Table 8). Similarly, the agricultural land category located in the central part of the parish decreased by 1.43% from pre-fire to post-fire scene. Nevertheless, the forest category behaves differently, with a growth of 3.7% in the Vilcabamba parish during the post-fire scene. The agricultural lands decreased from 13.54% (pre-fire) to 12.11% (post-fire). Also, urban zones concentrated in the central part of the study area increased by 0.1% from pre-fire to post-fire scene. Finally, the other land category rose from 0.32% in pre-fire to 2.04% in post-fire. Finally, water bodies increased from 0.33% in pre-fire to 0.49% in post-fire. The pre-fire and post-fire data for the fire perimeter show that the shrub and herbaceous vegetation category decreased by 7.19 ha in the post-fire scene. Additionally, the fact that there were no urban areas within the fire perimeter allowed a gradual recovery of vegetation two years after the fire.



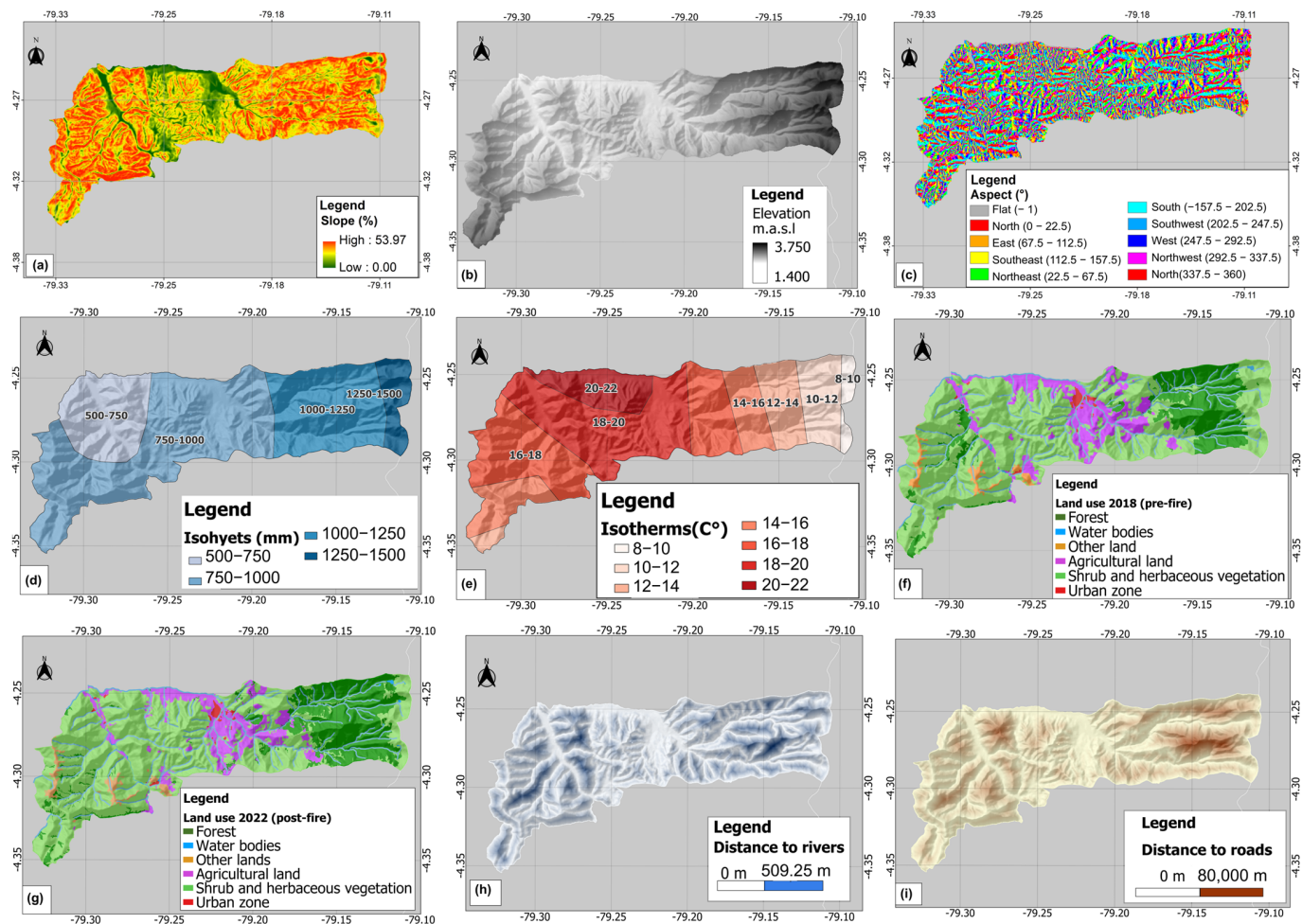


**Figure 10.** Variables for the wildfire susceptibility map: (a) slope angle; (b) elevation; (c) slope aspect; (d) isohyets; (e) isotherms; (f) land use in pre-fire scene; (g) land use in post-fire scene; (h) distance to water bodies (rivers); and (i) distance to roads. Source: Adapted from [60,61,64].

**Table 8.** Land use in pre- and post-fire scenes in Vilcabamba Parish compared to the wildfire perimeter. Source: Adapted from [60].

Class	Land Use Categories	Area in Vilcabamba Parish (ha)		Area in Wildfire Perimeter (ha)	
		Pre-Fire (2018)	Post-Fire (2022)	Pre-Fire (2018)	Post-Fire (2022)
1	Shrub and herbaceous vegetation	10,249.91	9846.52	1594.89	1587.70
2	Forest	3077.20	3652.00	119.04	123.35
3	Agricultural lands	2163.70	1935.83	4.81	6.79
4	Other lands	308.74	324.55	118.61	119.51
5	Urban zone	126.95	141.89	-	-
6	Water bodies	52.40	78.11	0.30	0.30

This study analysed the wildfire susceptibility in Vilcabamba Parish based on the Analytic Hierarchy Process (AHP). The principal outcomes confirmed that the wildfire perimeter exhibits 59.83% low–moderate fire susceptibility and 27.80% high fire susceptibility (Figure 11a). In general, the study area is a small area with null fire susceptibility (12.37%), located in the northeast of the parish (near the El Palto community and the Podocarpus National Park) and in the centre of the parish (urban areas). This section allowed us to understand the dynamics between vegetation and climate conditions, consid-

ering pre-fire and post-fire scenes, and to identify the influencing factors in the forest fire of 2019 in Vilcabamba parish. This analysis establishes the following: (i) the closest settlers to water bodies (lagoons and lakes) are the Capulí and El Palto, in the northwest zone of the study area (Figures S3 and 11b), (ii) rivers are closer to the firefighters in the event of a wildfire (Figures S4 and 11c), and (iii) the Tumianuma and Chulapo settlers are in more danger because they are a long way from lagoons and lakes.

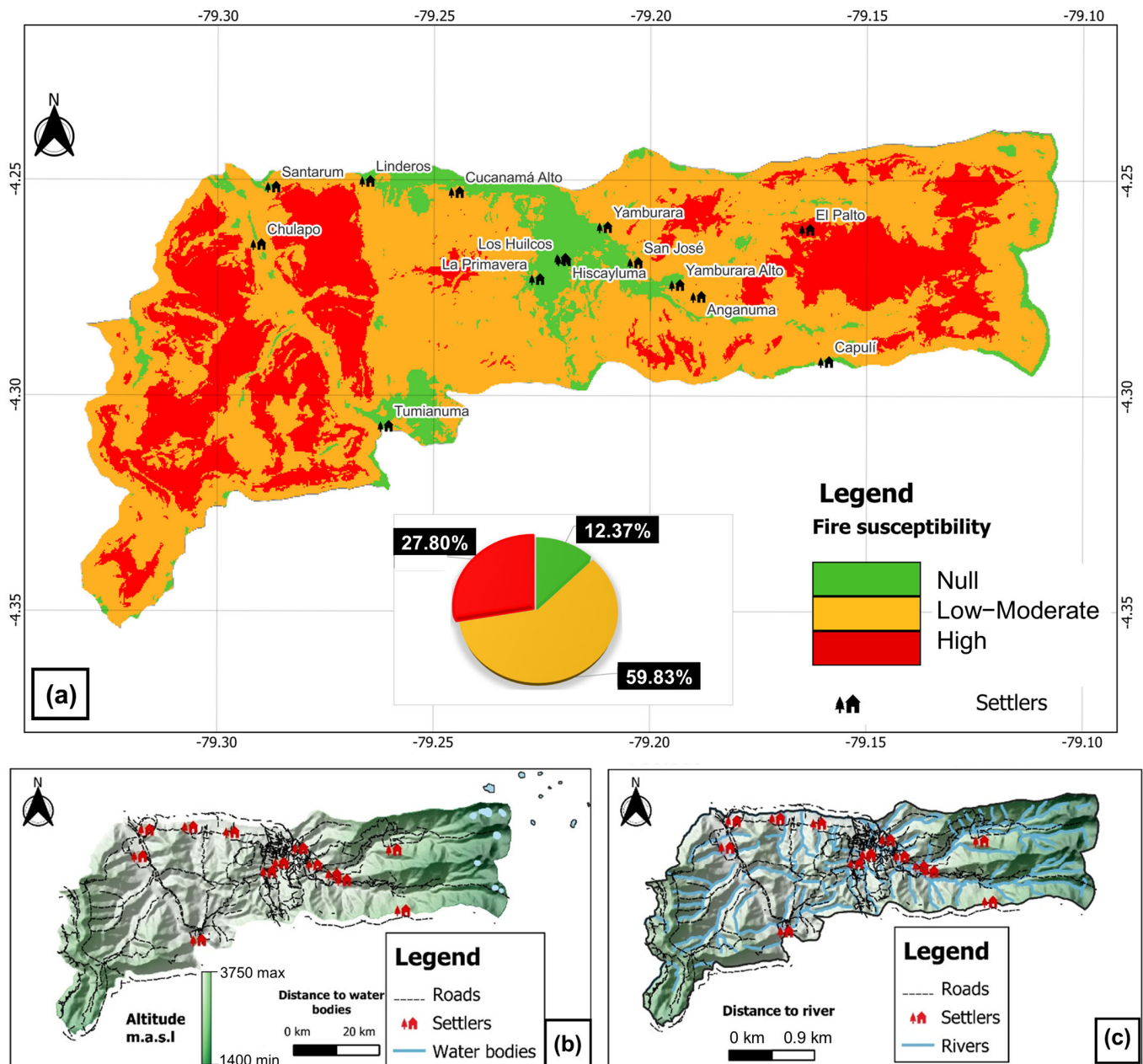


**Figure 11.** Analysis of fire susceptibility: (a) Wildfire susceptibility map through AHP method. (b) Access to water bodies (lagoons and lakes) by aerial transport for each parcel. (c) Access to rivers and streams by terrestrial transport.

#### 4.4. Proposal of Action Plan for Fire Management in Vilcabamba Parish

The proposal of a fire action plan in Vilcabamba parish includes the analysis of cartographic information to generate fire probability points and select six strategic refuge zones, as shown in Figure 12. For the selection of the five safety zones in wildfire events, we considered the location of health centres, fire stations, and the proximity of water bodies.

Meanwhile, for the selection of fire probability points and refuge zones, we used Dijkstra's shortest path algorithm [79] through the Road Graph plugin in QGIS framework and the location of historical fire points within the pre-fire scene, during the period 2011–2019, obtained from the SGNRE and VIIRS data, as well as the results of the fire susceptibility map. Furthermore, we distributed the safety zones in places close to the roads and population centres of Vilcabamba parish, following the escape routes to prevent the spread of the fire.

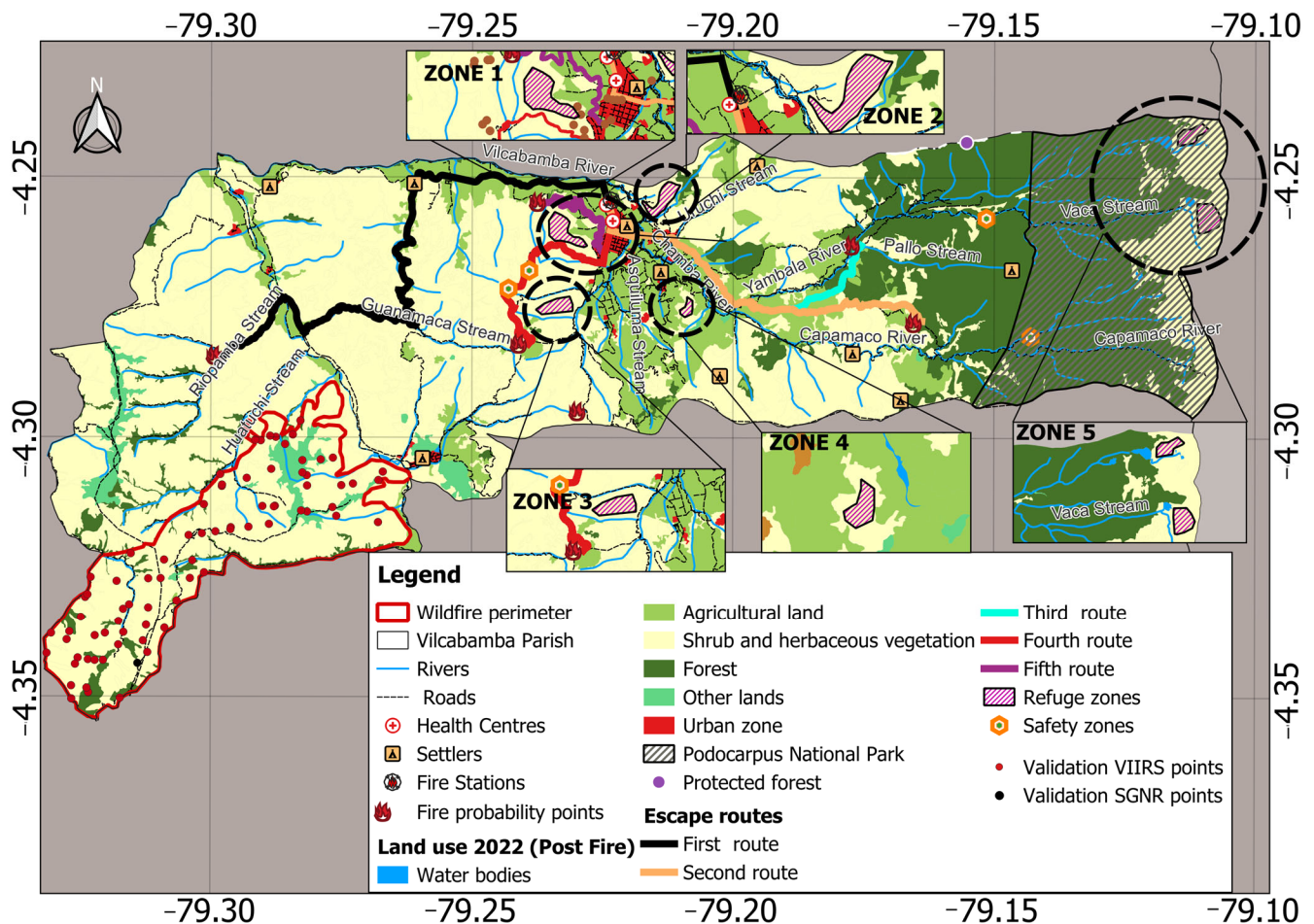


**Figure 12.** Proposal action plan in Vilcabamba parish where evacuation routes and fire refuge areas are outlined.

For the escape routes, we considered variables such as the proximity to water bodies (rivers, streams, lagoons and lakes), distance to roads and settlers to ensure accessibility, and a timely response to potential fire events. We included land use data in the post-fire scene for the representation of protected areas (Podocarpus National Park) and zones with vegetation coverage. We used the main road layer for accessibility information in the selection of the best escape routes. Finally, we included the settlers' location to know the distance to an urban zone that could be affected in case of fire. The settlers must be within a reasonable distance of water bodies, which act as natural barriers to manage the spreading of the wildfire. They must also enhance their capacity to avail themselves of this invaluable resource during firefighting efforts or as a means of evacuation if required. This action plan will allow us to comprehensively illustrate wildfire events, selecting the shortest and optimal escape routes in the event of a fire.

## 5. Discussion

GIS-based models (e.g., AHP method) have been widely applied for fire susceptibility [26,80]. However, an integral approach has not been recorded to consider these models



when developing a fire action plan. Therefore, this study highlights the importance of using remote sensing tools (e.g., spectral indices) and the AHP method to establish a fire action plan in the Andean region of Vilcabamba parish. The proposed fire action plan considered fires recorded in 2019 (pre-fire scene), fire hotspots from satellite data (VIIRS) in the fire perimeter of the study area, and a fire susceptibility model to delineate evacuation routes for firefighters to attend fire events within the study area and refuge zones with lower fire propagation. These methodologies allow us to establish a conceptual model for fire management and monitoring adapted to the particularities and needs of the Vilcabamba parish. The purpose is to contribute to decision making by the authorities and, at the same time, to be considered a preliminary study but one that can be applied to other regions with similar geographic–climatic conditions. Remote sensing tools are crucial in analysing preconditions, which can lead to a significant forest fire in Vilcabamba parish. Daily satellite scans also contribute to a vast dataset, enabling vegetation monitoring through time series analysis.

This study analysed the fire severity of the event of 3 September 2019. We analysed specifically the fire perimeter within the delineation of the Vilcabamba parish, located in the Andean region of Ecuador for several reasons: (i) the SNGRE recorded 87 historical events in the study area in the period 2011–2019 and 148 fire hotspots from VIIRS data, (ii) the availability of 78 fire validation points according to the VIIRS and SNGRE data in the year 2019 (pre-fire scene), (iii) the presence of the Podocarpus National Park and protected forest, in the northeast region of the parish, (iv) wind patterns that influence its mountainous topography and the prevailing regional weather patterns throughout the southern region, and (v) the drought conditions related to the increase in urban areas and the reduction in shrub and herbaceous vegetation evident in the post-fire scene. This area has evidence of a dry austral rainy season (from June to September), with rainfall lasting from December to April, extending into May.

In Ecuador, some analyses of wildfires used remote sensing techniques. For instance, in Imbabura province, a study provides comprehensive insights into the vegetation dynamics in a forest fire by applying NDVI values that show a significant decline in post-fire scenes [81]. Meanwhile, another study developed a replicable approach for semi-automatically detecting forest fires and evaluating vegetation recovery post-fire through Landsat 8 (OLI) imagery in Quilanga canton (Loja province) [82]. Moreover, in Chilla canton (El Oro province), a high performance of the NBRI (burned normalised index) identified the scar of the forest fire. Meanwhile, the NDVI determined a mean value of 0.15 showing low vegetation productivity [83]. Finally, a study in Chimborazo found that dNBR using Landsat imagery delimited the fire perimeter and showed a 55% similarity with the delineation of the national database [84].

Regarding multispectral imagery, this study showed that data obtained from Sentinel-2A are highly beneficial for identifying burned areas. For instance, a study on an island in the Aegean Sea (Greece) demonstrated the accuracy shared by Sentinel-2A and Landsat-8 by showing the high exactitude of the Sentinel-2A to map fire scars and the excellent performance of the NIR and mid-infrared bands of both sensors [85]. On the other hand, Lo Conti et al. [86] found a high bias in the surface analysis concerning cloudy and water body pixels in Sicily, Italy.

In this study, we use the cloud-gap-filled (CGF) method to fully fill data gaps in Sentinel-2A imagery of the NDVI in the period 2016–2022. This analysis allowed a better understanding of the dynamics of vegetation recovery in pre-fire and post-fire scenes by considering monthly data that allow us to relate this to the sector's climatology and fire frequency incidence. The CGF method for NDVI time series is a widely used tool worldwide because it provides a bi-temporal analysis using satellite data that encompass several factors such as phenology, climate change, and geological-natural risk assessments [87]. According to Karlsen et al. [20], the time series vegetation index accurately depended on the atmospheric conditions instead of being highly structured, as shown in their study in Central Spitsbergen, Svalbard. Their findings showed extreme bias in 2018, where

the algorithm had low detection. In the same way, the 2017 scene for Vilcabamba parish showed a low detection problem due to cloudiness. Still, the rest of the time series had an exceptional performance.

The outcomes in the vegetation recovery in the wildfire perimeter using the NDVI showed 9.63% in the low vegetation productivity category on the post-fire scene in 2019 and 0.99% for the post-fire scene, after a two-year recovery period (2021), showing the vegetation recovery in the region. However, the NBR index in the post-fire scene (2019) showed that the Vilcabamba parish presented 3.48% in high vegetation regrowth and 16.58% for the post-fire scene (2021). The effects of climate change in the study area include the predominant frequency of fires in dry periods, showing that, as precipitation decreases, temperatures rise significantly.

The Analytic Hierarchy Process (AHP) method applied in the Vilcabamba parish revealed that most settlers exhibit moderate fire probability, verified by SNGRE data, which indicates that the wildfire perimeter exhibits a high susceptibility to fire. Similarly, other regions, such as the states of Kashmir (JK), Himachal Pradesh (HP), and Uttarakhand (UK) of India demonstrated a moderate wildfire probability [88]. On the other hand, a study in the Andean region in Ibarra (Ecuador) delineated areas within the paramo ecosystem exhibiting low fire severity, attributable to low temperatures and challenging accessibility [65].

### 5.1. The Main Trends in the Results

This study identified the safety zones through the action plan for wildfire management that designates strategic areas according to the proximity to rivers, streams, water bodies (i.e., lakes, lagoons), and roads for impeding the kinetic energy of fire propagation. We used historical records of wildfires in Vilcabamba parish from the SNGRE and VIIRS data to define the shortest escape routes given the probability of fire occurrence. For escape route identification, we used the Road graph plugin that uses Dijkstra's shortest path algorithm. The safety zones could enhance the effectiveness of fire management and containment efforts, considering the strategic position of firefighting resources to ensure a swift and efficient response to any wildfire within the region. Similarly, in western New Mexico, western Wyoming, and Northern California they used a GEE tool to delineate safety zones, allowing the users to draw a polygon of potential safety zones based on slope, wind, and fire conditions [89]. In the same way, Debnath, P.A. [90] used the shortest path tool to aim for the best route to respond to a medical emergency in India, indicating that the Road graph plugin shows that the shortest route is 41.75 km long, considering information about roads and junctions. The forest fire warning system should include surface water and groundwater (aquifer) management. Stable isotope techniques and the study of sociohydrology makes it possible to monitor water quality and consider the human–environment system, which is vital for the sustainability of natural resources [91].

### 5.2. Methodological Limitations

We identified the following limitations: (i) the high cloudiness, due to its Andean region, affected index results within the study area and proved to be a significant challenge, adversely impacting the time series and vegetation index analysis; (ii) the proposal plan focused on a specific point of wildfire probability; and (iii) practical challenges in the proposal action plan such as land use conflicts, funding constraints, and community engagement issues.

### 5.3. Implications of the Results and Avenues for Future Research

For future studies, it is recommended that automatised fire georeferenced points are implemented and the closest escape route is drawn for the action plan. This study also suggests effective stakeholder coordination and adaptive management approaches for overcoming the practical challenges in the development of the action plan for fire management. This study recognises the implementation of machine learning tools that



exhibit significant potential as a future research topic, contributing to identifying high-probability areas with unparalleled accuracy. However, it is crucial to note that the efficacy of these methods is contingent upon the quality of data obtained from satellites, a factor often hindered by cloud cover in most cases.

## 6. Conclusions

This study evaluated forest fire severity in Vilcabamba parish, Ecuador, on 3 September 2019, using the NBR, NDVI, dNDVI and dNBR indices, revealing that vegetation recovery depends on fire severity and anthropogenic activities in the area. Complementarily, we implemented a multi-criteria model for fire susceptibility, considering slope angle, slope aspect, elevation, distance to roads, distance to rivers, land use, isotherms and isohyets. The AHP approach compared fire severity models (dNDVI and dNBR) for mapping burned areas and vegetation recovery, providing a robust fire prevention and planning framework. These models were validated with statistical algorithms, proving their accuracy and functioning as critical criteria for the proposed action plan for fire management. The integrated approach of this article highlights the importance of implementing specific restoration strategies that provide a framework for post-fire management. The methodology applied can be replicated in regions with similar climates and socio-economic conditions.

The dNDVI and dNBR models explain wildfire dynamics over time for a more nuanced assessment of fire severity and its impacts on natural ecosystems by considering bi-temporal scenarios. This study implements GEE's cloud-based platform to calculate spectral indices and streamline the data processing and analysis workflow. Its rapid computation of indices facilitates timely decision making and management actions. We combined the fire severity models and the GIS-based approach (AHP model) to establish a fire action plan that enhances the effectiveness of wildfire management efforts. This article provides a framework for decision making in preventing and mitigating wildfires, facilitating stakeholder coordination, and implementing targeted interventions.

The NDVI and NBR showed a notable correlation, offering technical insights into conditions preceding fire events and encompassing vegetation regrowth patterns. The wildfire perimeter exhibited 25.7% of vegetation regrowth. Pixels derived from the pre-fire NDVI covered 3076.21 ha (Figure 6), while the NBR index amounted to 1018.56 ha, indicating burned areas characterised as moderate-to-low severity (Figure 5). For the time series of the NDVI, we used the cloud-gap-filled method for filling gaps in data for a more precise analysis of the wildfire dynamics (Figure S2). The NDMI showed that 55% of Vilcabamba parish shows a high water stress and only 1.26% with a very high canopy cover or no water stress (Figure 6).

The wildfire susceptibility model provides valuable insights into the spatial distribution of the fire, enabling targeted interventions in high-risk areas (Figure 11). The AHP method integrates diverse factors and prioritises adaptation efforts, enhancing the resilience of communities and ecosystems against the threat of wildfires, and it was verified with SNGRE field data, capturing the temporal evolution of fire events and their associated environmental variables.

The proposed action plan included the optimal escape routes and five refuge zones that help the group of firefighters as it enables them to identify the nearest river or water body (lake or lagoon) for decision-makers that could provide water for fire mitigation by air or land transport (Figure 12). This analysis considered climate, topographic conditions (altitudes from 1400 to 3750 m.a.s.l.), and less densely populated areas conducive to mitigating the wildfire spread. This methodology offers governmental and institutional authorities the preliminary conceptual model (Figure 4) to protect these designated areas, as an approach adaptable to places with similar geographic conditions.

**Supplementary Materials:** The following supporting information can be downloaded at <https://www.mdpi.com/article/10.3390/f15122210/s1>, Figure S1: Original NDVI time series before applying gap-filled method; Figure S2: Gap-filled NDVI Times series in Vilcabamba parish during 2016–2022 [73]; Figure S3: Distance to water bodies (lagoons and lakes) with respect to settlements

located in Vilcabamba parish; Figure S4: Distance to rivers and streams (intermittent and perennial) with respect to settlements located in Vilcabamba parish.

**Author Contributions:** Conceptualization, F.T., A.G., F.G., L.B.-M. and F.M.-C.; methodology, A.G., F.G., C.B.-S., L.B.-M. and F.M.-C.; software, F.G. and L.B.-M.; validation, F.G. and L.B.-M.; formal analysis, L.B.-M. and F.M.-C.; investigation, F.T., A.G., F.G., C.B.-S., L.B.-M. and F.M.-C.; resources, A.G., F.G. and L.B.-M.; data curation, F.G.; writing—original draft preparation, F.T., A.G., F.G., L.B.-M. and F.M.-C.; writing—review and editing, F.T., A.G., F.G., C.B.-S., F.M.-C. and L.B.-M.; visualisation, F.G. and L.B.-M.; supervision, F.M.-C. and L.B.-M.; project administration, F.T.; funding acquisition, F.T. All authors have read and agreed to the published version of the manuscript.

**Funding:** This research received dissemination support from the Centre of Studies in Geography and Spatial Planning (CEGOT), funded by national funds through the Foundation for Science and Technology (FCT) under the reference UIDB/04084/2020.

**Data Availability Statement:** Data are contained within the article and Supplementary Materials.

**Acknowledgments:** The authors thank the Ing. Paúl Carrión-Mero, from research centre CIPAT-ESPOL, for his guidance and support and the following projects: “Registro del Patrimonio Geológico y Minero y su incidencia en la defensa y preservación de la geodiversidad en Ecuador” (Registry of Geological and Mining Heritage and its impact on the defence and preservation of geodiversity in Ecuador), with code No. CIPAT-01-2018 from the ESPOL Polytechnic University, and “Monitoreo de áreas susceptibles a incendios forestales y de zonas prioritarias de prevención del cantón Loja” (Monitoring of areas susceptible to forest fires and priority prevention areas of the Loja canton), with code No. 46-DI-FARNR-2023, from the Nacional University of Loja (UNL, Spanish acronym). We also thank the Researcher Paulo Escandón-Panchana, for his collaboration in this study. We also thank to the reviewers and editor.

**Conflicts of Interest:** The authors declare no conflicts of interest.

## References

1. Camarero, J.J.; Guijarro, M.; Calama, R.; Valeriano, C.; Pizarro, M.; Madrigal, J. Wildfires Improve Forest Growth Resilience to Drought. *Fire* **2023**, *6*, 161. [\[CrossRef\]](#)
2. De Frenne, P.; Lenoir, J.; Luoto, M.; Scheffers, B.R.; Zellweger, F.; Aalto, J.; Ashcroft, M.B.; Christiansen, D.M.; Decocq, G.; De Pauw, K.; et al. Forest microclimates and climate change: Importance, drivers and future research agenda. *Glob. Change Biol.* **2021**, *27*, 2279–2297. [\[CrossRef\]](#) [\[PubMed\]](#)
3. Spies, T.A.; White, E.M.; Kline, J.D.; Fischer, A.P.; Ager, A.; Bailey, J.; Bolte, J.; Koch, J.; Platt, E.; Olsen, C.S.; et al. Examining fire-prone forest landscapes as coupled human and natural systems. *Ecol. Soc.* **2014**, *19*, 9. [\[CrossRef\]](#)
4. Martínez, J.; Vega-García, C.; Chuvieco, E. Human-caused wildfire risk rating for prevention planning in Spain. *J. Environ. Manag.* **2009**, *90*, 1241–1252. [\[CrossRef\]](#) [\[PubMed\]](#)
5. Carrión-Paladines, V.; Correa-Quezada, L.; Valdiviezo Malo, H.; Zurita Ruáles, J.; Pereddo Tumbaco, A.; Zambrano Pisco, M.; Lucio Panchi, N.; Jiménez Álvarez, L.; Benítez, Á.; Loján-Córdova, J. Exploring the ethnobiological practices of fire in three natural regions of Ecuador, through the integration of traditional knowledge and scientific approaches. *J. Ethnobiol. Ethnomed.* **2024**, *20*, 60. [\[CrossRef\]](#)
6. Frago, P.; Corona, A.P.; Hernández, B.P. Efecto del Fuego Sobre las Propiedades de los Suelos Agrícolas en la Zona Kárstica del sur de Quintana Roo. *Eur. Sci. J. ESJ* **2022**, *11*, 406. [\[CrossRef\]](#)
7. Ibrahim, S.; Kose, M.; Adamu, B.; Jega, I.M. Remote sensing for assessing the impact of forest fire severity on ecological and socio-economic activities in Kozan District, Turkey. *J. Environ. Stud. Sci.* **2024**, *14*, 13. [\[CrossRef\]](#)
8. Bolotin, L.A.; McMillan, H. A hydrologic signature approach to analysing wildfire impacts on overland flow. *Hydrol. Process.* **2024**, *38*, e15215. [\[CrossRef\]](#)
9. Schweizer, D.; Preisler, H.; Entwistle, M.; Gharibi, H.; Cisneros, R. Using a Statistical Model to Estimate the Effect of Wildland Fire Smoke on Ground Level PM2.5 and Asthma in California, USA. *Fire* **2023**, *6*, 159. [\[CrossRef\]](#)
10. Grünig, M.; Seidl, R.; Senf, C. Increasing aridity causes larger and more severe forest fires across Europe. *Glob. Change Biol.* **2023**, *29*, 1648–1659. [\[CrossRef\]](#)
11. Stoddard, M.T.; Huffman, D.W.; Fulé, P.Z.; Crouse, J.E.; Sánchez Meador, A.J. Forest structure and regeneration responses 15 years after wildfire in a ponderosa pine and mixed-conifer ecotone, Arizona, USA. *Fire Ecol.* **2018**, *14*, 12. [\[CrossRef\]](#)
12. Kganyago, M.; Shikwambana, L. Assessment of the characteristics of recent major wildfires in the USA, Australia and Brazil in 2018–2019 using multi-source satellite products. *Remote Sens.* **2020**, *12*, 1803. [\[CrossRef\]](#)
13. Ribeiro, L.M.; Rodrigues, A.; Lucas, D.; Viegas, D.X. The impact on structures of the Pedrógão Grande fire complex in June 2017 (Portugal). *Fire* **2020**, *3*, 57. [\[CrossRef\]](#)

14. Ramos Rodríguez, M.P.; Poma Cabrera, E.B.; Reyes Chancay, J.E. Estadísticas de incendios forestales en el cantón Loja, provincia Loja, Ecuador, en el periodo 2011–2020. *Bosques Latid. Cero* **2024**, *14*, 64–76. [\[CrossRef\]](#)
15. Reyes-Bueno, F.; Loján-Córdova, J. Assessment of Three Machine Learning Techniques with Open-Access Geographic Data for Forest Fire Susceptibility Monitoring—Evidence from Southern Ecuador. *Forests* **2022**, *13*, 474. [\[CrossRef\]](#)
16. Sarango, J.; Muñoz, J.; Muñoz, L.; Zhofre, A. Impacto ecológico de un incendio forestal en la flora del páramo antrópico del Parque Universitario “Francisco Vivar Castro”, Loja, Ecuador. *Bosques Latid. Cero* **2019**, *9*, 101–114.
17. Rodríguez, M.; Muñoz, C. *Fundamentos de la Climatología*, 2nd ed.; Universidad de la Rioja: Madrid, Spain, 2012; ISBN 978-84-695-2799-3.
18. Roerink, G.J.; Menenti, M.; Verhoef, W. Reconstructing cloudfree NDVI composites using Fourier analysis of time series. *Int. J. Remote Sens.* **2000**, *21*, 1911–1917. [\[CrossRef\]](#)
19. Pham, V.T.; Do, T.A.T.; Tran, H.D.; Do, A.N.T. Classifying forest cover and mapping forest fire susceptibility in Dak Nong province, Vietnam utilizing remote sensing and machine learning. *Ecol. Inform.* **2024**, *79*, 102392. [\[CrossRef\]](#)
20. Karlsen, S.R.; Stendardi, L.; Tømmervik, H.; Nilsen, L.; Arntzen, I.; Cooper, E.J. Time-series of cloud-free sentinel-2 NDVI data used in mapping the onset of growth of central Spitsbergen, Svalbard. *Remote Sens.* **2021**, *13*, 3031. [\[CrossRef\]](#)
21. Mateo-García, G.; Gómez-Chova, L.; Amorós-López, J.; Muñoz-Marí, J.; Camps-Valls, G. Multitemporal Cloud Masking in the Google Earth Engine. *Remote Sens.* **2018**, *10*, 1079. [\[CrossRef\]](#)
22. Xue, J.; Su, B. Significant Remote Sensing Vegetation Indices: A Review of Developments and Applications. *J. Sens.* **2017**, *2017*, 1353691. [\[CrossRef\]](#)
23. Sruthi, S.; Aslam, M.A.M. Agricultural Drought Analysis Using the NDVI and Land Surface Temperature Data; a Case Study of Raichur District. *Aquat. Procedia* **2015**, *4*, 1258–1264. [\[CrossRef\]](#)
24. Phan, P.; Chen, N.; Xu, L.; Dao, D.M.; Dang, D. NDVI variation and yield prediction in growing season: A case study with tea in Tanuyen Vietnam. *Atmosphere* **2021**, *12*, 962. [\[CrossRef\]](#)
25. Keeley, J.E. Fire intensity, fire severity and burn severity: A brief review and suggested usage. *Int. J. Wildl. Fire* **2009**, *18*, 116. [\[CrossRef\]](#)
26. Sandoya, V.; Saura-Mas, S.; Granzow-de la Cerda, I.; Arellano, G.; Macía, M.J.; Tello, J.S.; Lloret, F. Contribution of species abundance and frequency to aboveground forest biomass along an Andean elevation gradient. *For. Ecol. Manag.* **2021**, *479*, 118549. [\[CrossRef\]](#)
27. Chemweno, P.; Pintelon, L.; Van Horenbeek, A.; Muchiri, P. Development of a risk assessment selection methodology for asset maintenance decision making: An analytic network process (ANP) approach. *Int. J. Prod. Econ.* **2015**, *170*, 663–676. [\[CrossRef\]](#)
28. SNGRE. *Informe de Situación No.39. Incendios Forestales a Nivel Nacional del 2019 en Ecuador*; Secretaría Nacional de Gestión de Riesgos y Emergencias (SNGRE): Quito, Ecuador, 2019.
29. MAE. National System of Protected Areas. Available online: <http://areasprotegidas.ambiente.gob.ec/mapa> (accessed on 28 October 2024).
30. Municipio de Loja. Incendios Forestales del 2019. Available online: <https://www.loja.gob.ec/noticia/2019-10/incendios-forestales-del-fin-de-semana-fueron-provocados> (accessed on 22 November 2023).
31. SGNRE. *Reporte de Monitoreo de Amenazas y Eventos Peligrosos No. 0682*; Secretaría Nacional de Gestión de Riesgos y Emergencias (SNGRE): Samborondón, Ecuador, 2023.
32. INEC. Cuestionario Censal 2022. Available online: <https://www.ecuadorencifras.gob.ec/institucional/home/> (accessed on 17 October 2024).
33. GAD Parroquial Vilcabamba. *Plan de Ordenamiento Territorial (PDOT) Vilcabamba 2019–2023*; Gobierno Autónomo Descentralizado de la Parroquial Vilcabamba: Loja, Ecuador, 2019.
34. Chen, D.; Chen, H.W. Using the Köppen classification to quantify climate variation and change: An example for 1901–2010. *Environ. Dev.* **2013**, *6*, 69–79. [\[CrossRef\]](#)
35. Díaz, S.C.; Quezada, L.C.; Álvarez, L.J.; Loján-Córdova, J.; Carrión-Paladines, V. Indigenous use of fire in the paramo ecosystem of southern Ecuador: A case study using remote sensing methods and ancestral knowledge of the Kichwa Saraguro people. *Fire Ecol.* **2023**, *19*, 5. [\[CrossRef\]](#)
36. Primicias Incendio Forestal en Cantón Quilanga en la Provincia de Loja. Available online: <https://www.primicias.ec/sociedad/incendio-forestal-loja-avanza-pese-labores-contencion-77186/> (accessed on 30 October 2024).
37. Reyes-Bueno, F.; Tubío Sánchez, J.; Gracia Samaniego, J.; Miranda Barrós, D.; Crecente Maseda, R.; Sánchez-Rodríguez, A. Factors influencing land fractioning in the context of land market deregulation in Ecuador. *Land Use Policy* **2016**, *52*, 144–150. [\[CrossRef\]](#)
38. Lastovicka, J.; Svec, P.; Paluba, D.; Kobliuk, N.; Svoboda, J.; Hladky, R.; Stych, P. Sentinel-2 data in an evaluation of the impact of the disturbances on forest vegetation. *Remote Sens.* **2020**, *12*, 1914. [\[CrossRef\]](#)
39. Velastegui-Montoya, A.; Montalván-Burbano, N.; Carrión-Mero, P.; Rivera-Torres, H.; Sadeck, L.; Adami, M. Google Earth Engine: A Global Analysis and Future Trends. *Remote Sens.* **2023**, *15*, 3675. [\[CrossRef\]](#)
40. ESA Copernicus Open Access Hub. Available online: <https://scihub.copernicus.eu/> (accessed on 16 April 2024).
41. Huang, C.; Zhang, C.; He, Y.; Liu, Q.; Li, H.; Su, F.; Liu, G.; Bridhikitti, A. Land cover mapping in cloud-prone tropical areas using Sentinel-2 data: Integrating spectral features with NDVI temporal dynamics. *Remote Sens.* **2020**, *12*, 1163. [\[CrossRef\]](#)
42. Jodhani, K.H.; Patel, H.; Soni, U.; Patel, R.; Valodara, B.; Gupta, N.; Patel, A.; Omar, P.J. Assessment of forest fire severity and land surface temperature using Google Earth Engine: A case study of Gujarat State, India. *Fire Ecol.* **2024**, *20*, 23. [\[CrossRef\]](#)

43. Praticò, S.; Solano, F.; Di Fazio, S.; Modica, G. Machine Learning Classification of Mediterranean Forest Habitats in Google Earth Engine Based on Seasonal Sentinel-2 Time-Series and Input Image Composition Optimisation. *Remote Sens.* **2021**, *13*, 586. [CrossRef]
44. Filgueiras, R.; Mantovani, E.C.; Althoff, D.; Fernandes Filho, E.I.; da Cunha, F.F. Crop NDVI Monitoring Based on Sentinel 1. *Remote Sens.* **2019**, *11*, 1441. [CrossRef]
45. Hudak, A.T.; Morgan, P.; Bobbitt, M.J.; Smith, A.M.S.; Lewis, S.A.; Lentile, L.B.; Robichaud, P.R.; Clark, J.T.; McKinley, R.A. The Relationship of Multispectral Satellite Imagery to Immediate Fire Effects. *Fire Ecol.* **2007**, *3*, 64–90. [CrossRef]
46. Easterday, K.; Kislik, C.; Dawson, T.; Hogan, S.; Kelly, M. Remotely Sensed Water Limitation in Vegetation: Insights from an Experiment with Unmanned Aerial Vehicles (UAVs). *Remote Sens.* **2019**, *11*, 1853. [CrossRef]
47. Huete, A.R. Vegetation Indices, Remote Sensing and Forest Monitoring. *Geogr. Compass* **2012**, *6*, 513–532. [CrossRef]
48. Deng, G.; Tang, Z.; Dong, C.; Shao, D.; Wang, X. Development and Evaluation of a Cloud-Gap-Filled MODIS Normalized Difference Snow Index Product over High Mountain Asia. *Remote Sens.* **2024**, *16*, 192. [CrossRef]
49. Cryer, J.D.; Chan, K.-S. *Time Series Analysis*, 2nd ed.; Springer Texts in Statistics; Springer: New York, NY, USA, 2008; ISBN 978-0-387-75958-6.
50. Verger, A.; Sánchez-Zapero, J.; Weiss, M.; Descals, A.; Camacho, F.; Lacaze, R.; Baret, F. GEOV2: Improved smoothed and gap filled time series of LAI, FAPAR and FCover 1 km Copernicus Global Land products. *Int. J. Appl. Earth Obs. Geoinf.* **2023**, *123*, 103479. [CrossRef]
51. Gandhi, U. JavaScript and the Earth Engine API. In *Cloud-Based Remote Sensing with Google Earth Engine*; Springer International Publishing: Cham, Switzerland, 2024; pp. 3–18.
52. Saaty, T.L. Decision making—The Analytic Hierarchy and Network Processes (AHP/ANP). *J. Syst. Sci. Syst. Eng.* **2004**, *13*, 1–35. [CrossRef]
53. Millet, I.; Wedley, W.C. Modelling risk and uncertainty with the analytic hierarchy process. *J. Multi-Criteria Decis. Anal.* **2002**, *11*, 97–107. [CrossRef]
54. Caner, H.I.; Aydin, C.C. Shipyard site selection by raster calculation method and AHP in GIS environment, İskenderun, Turkey. *Mar. Policy* **2021**, *127*, 104439. [CrossRef]
55. Singh, B. Analytical hierarchical process (AHP) and fuzzy AHP applications—A review paper. *Int. J. Pharm. Technol.* **2016**, *8*, 4925–4946.
56. Salmeron, J.L.; Smarandache, F. Redesigning Decision Matrix Method with an indeterminacy-based inference process. *Int. J. Appl. Math. Stat.* **2008**, *13*, 4–11.
57. Menon, R.R.; Vijayakumar, R.; Pandey, J.K. Selection of Optimal Air Independent Propulsion System using Forced Decision Matrix. *Def. Sci. J.* **2020**, *70*, 103–109. [CrossRef]
58. Reyes-Bueno, F.; Balcazar-Gallegos, C. Factores que inciden en la probabilidad de ocurrencia de incendios forestales en Ecuador. *FIGEMPA Investig. Desarro.* **2021**, *11*, 50–60. [CrossRef]
59. Vadrevu, K.P.; Eaturu, A.; Badarinath, K.V.S. Fire risk evaluation using multicriteria analysis—a case study. *Environ. Monit. Assess.* **2010**, *166*, 223–239. [CrossRef]
60. MAE Metadatos del Ministerio de Ambiente, Agua y Transición Ecológica del Ecuador. Available online: <http://ide.ambiente.gob.ec/mapainteractivo/> (accessed on 22 September 2023).
61. UNL Estaciones Meteorológicas en la Ciudad de Loja. Available online: <https://geoportal.unl.edu.ec/visor-climatico/visor/> (accessed on 22 January 2024).
62. INAHMI Estaciones Meteorológicas del Ecuador. Available online: <https://www.inamhi.gob.ec/> (accessed on 24 May 2024).
63. Sahana, M.; Ganaie, T.A. GIS-based landscape vulnerability assessment to forest fire susceptibility of Rudraprayag district, Uttarakhand, India. *Environ. Earth Sci.* **2017**, *76*, 676. [CrossRef]
64. IGM Modelo Digital del Terreno de Ecuador a Escala 1:50,000. Available online: <https://www.datosabiertos.gob.ec/dataset/modelo-digital-del-terreno> (accessed on 14 December 2023).
65. Arias, P.; Cabrera, S.; Jácome, G.; Arias-Muñoz, P.; Cabrera-García, S.; Jácome-Aguirre, G. A Multicriteria Geographic Information System Analysis of Wildfire Susceptibility in the Andean Region: A Case Study in Ibarra, Ecuador. *Fire* **2024**, *7*, 81. [CrossRef]
66. Mariscal, S.; Ríos, M.; Soria, F. Multicriteria analysis for identifying forest fire risk zones in the Biological Reserve of the Sama Cordillera, Bolivia. *Int. Arch. Photogramm. Remote Sens. Spat. Inf. Sci.* **2020**, *XLII-3/W12*, 113–118. [CrossRef]
67. IGM Visor de Datos Geográficos Oficiales de Ecuador. Base Continúa a Escala 1:50,000. Formato Shapefile. Available online: <https://www.geoportaligm.gob.ec/portal/index.php/visualizador/> (accessed on 27 January 2024).
68. Van Hoang, T.; Chou, T.Y.; Fang, Y.M.; Nguyen, N.T.; Nguyen, Q.H.; Xuan Canh, P.; Ngo Bao Toan, D.; Nguyen, X.L.; Meadows, M.E.; Canh, P.X.; et al. Mapping Forest Fire Risk and Development of Early Warning System for NW Vietnam Using AHP and MCA/GIS Methods. *Appl. Sci.* **2020**, *10*, 4348. [CrossRef]
69. Vilar del Hoyo, L.; Martín Isabel, M.P.; Martínez Vega, F.J. Logistic regression models for human-caused wildfire risk estimation: Analysing the effect of the spatial accuracy in fire occurrence data. *Eur. J. For. Res.* **2011**, *130*, 983–996. [CrossRef]
70. Poulos, H.M.; Barton, A.M.; Koch, G.W.; Kolb, T.E.; Thode, A.E. Wildfire severity and vegetation recovery drive post-fire evapotranspiration in a southwestern pine-oak forest, Arizona, USA. *Remote Sens. Ecol. Conserv.* **2021**, *7*, 579–591. [CrossRef]
71. Pang, S.E.H.; Slik, J.W.F.; Zurell, D.; Webb, E.L. The clustering of spatially associated species unravels patterns in tropical tree species distributions. *Ecosphere* **2023**, *14*, e4589. [CrossRef]



72. Silva-Souza, K.J.P.; Pivato, M.G.; Silva, V.C.; Haidar, R.F.; Souza, A.F. New patterns of the tree beta diversity and its determinants in the largest savanna and wetland biomes of South America. *Plant Divers.* **2023**, *45*, 369–384. [\[CrossRef\]](#)
73. Daniel, C.B.; Mathew, S.; Subbarayan, S. GIS-Based Study on the Association Between Road Centrality and Socio-demographic Parameters: A Case Study. *J. Geovis. Spat. Anal.* **2022**, *6*, 1. [\[CrossRef\]](#)
74. Murillo-Sandoval, P.; Hilker, T.; Krawchuk, M.; Van Den Hoek, J. Detecting and Attributing Drivers of Forest Disturbance in the Colombian Andes Using Landsat Time-Series. *Forests* **2018**, *9*, 269. [\[CrossRef\]](#)
75. Morante-Carballo, F.; Gurumendi-Noriega, M.; Cumbe-Vásquez, J.; Bravo-Montero, L.; Carrión-Mero, P. Georesources as an Alternative for Sustainable Development in COVID-19 Times—A Study Case in Ecuador. *Sustainability* **2022**, *14*, 7856. [\[CrossRef\]](#)
76. Franco, M.G.; Mundo, I.A.; Veblen, T.T. Field-Validated Burn-Severity Mapping in North Patagonian Forests. *Remote Sens.* **2020**, *12*, 214. [\[CrossRef\]](#)
77. Ritter, A.; Muñoz-Carpena, R. Performance evaluation of hydrological models: Statistical significance for reducing subjectivity in goodness-of-fit assessments. *J. Hydrol.* **2013**, *480*, 33–45. [\[CrossRef\]](#)
78. Tong, S.T.Y. The use of non-metric multidimensional scaling as an ordination technique in resource survey and evaluation: A case study from southeast Spain. *Appl. Geogr.* **1992**, *12*, 243–260. [\[CrossRef\]](#)
79. Chadha, C.; Garg, S. Shortest Path Analysis on Geospatial Data Using PgRouting: Visualization of Shortest Path on Road Network. In *International Conference on Innovative Computing and Communications, Proceedings of the ICICC 2018, Delhi, India, 5–6 May 2018*; Springer: Singapore, 2019; pp. 201–214.
80. Ahmadi, M.; Jorfi, S.; Kujlu, R.; Ghafari, S.; Darvishi Cheshmeh Soltani, R.; Jaafarzadeh Haghighifard, N. A novel salt-tolerant bacterial consortium for biodegradation of saline and recalcitrant petrochemical wastewater. *J. Environ. Manag.* **2017**, *191*, 198–208. [\[CrossRef\]](#)
81. Morante, F.; Bravo-Montero, L.; Carrión, P.; Velastegui, A.; Berrezueta, E. Forest Fire Assessment Using Remote Sensing to Support the Development of an Action Plan Proposal in Ecuador. *Remote Sens.* **2022**, *14*, 1783. [\[CrossRef\]](#)
82. Zhiminaicela Cabrera, J.B.; Quevedo-Guerrero, J.N.; León-Salto, M.B.; Mora-Encalada, C.P. Algoritmo Semiautomático para Mapear Incendios Forestales y Estimar la Recuperación Vegetal Mediante Imágenes Landsat-8. *Rev. Tecnol.-ESPOL* **2020**, *32*, 35–42. [\[CrossRef\]](#)
83. Zhiminaicela Cabrera, J.B.; Lima Morales, K.A.; Quevedo Guerrero, J.N.; García Batista, R.M.; Rogel Jarrín, B.A. Incendios forestales un factor influyente en la degradación de la biodiversidad del cantón Chilla, Ecuador. *Rev. Cient. Amaz.* **2021**, *4*, 5–12. [\[CrossRef\]](#)
84. Cisneros, C.; Calahorrano, J.; Abarca, M.; Manzano, M. Semiautomatic detection of burnt areas in Chimborazo-Ecuador using dNBR mean composites with adjusted thresholds. *Rev. Teledetec.* **2023**, *2023*, 89–99. [\[CrossRef\]](#)
85. Sdraka, M.; Dimakos, A.; Malounis, A.; Ntasiou, Z.; Karantzalos, K.; Michail, D.; Papoutsis, I. FLOGA: A Machine-Learning-Ready Dataset, a Benchmark, and a Novel Deep Learning Model for Burnt Area Mapping with Sentinel-2. *IEEE J. Sel. Top. Appl. Earth Obs. Remote Sens.* **2024**, *17*, 7801–7824. [\[CrossRef\]](#)
86. Lo Conti, F.; Hsu, K.-L.; Noto, L.V.; Sorooshian, S. Evaluating several satellite precipitation estimates and global ground-based dataset on Sicily (Italy). In *Remote Sensing for Agriculture, Ecosystems, and Hydrology XIV, Proceedings of the SPIE Remote Sensing, Edinburgh, UK, 24–27 September 2012*; Neale, C.M.U., Maltese, A., Eds.; SPIE: Bellingham, WA, USA, 2012; p. 853106.
87. Wang, C.; Zhang, H.; Wu, X.; Yang, W.; Shen, Y.; Lu, B.; Wang, J. AUTS: A Novel Approach to Mapping Winter Wheat by Automatically Updating Training Samples Based on NDVI Time Series. *Agriculture* **2022**, *12*, 817. [\[CrossRef\]](#)
88. Pragma; Kumar, M.; Tiwari, A.; Majid, S.I.; Bhadwal, S.; Sahu, N.; Verma, N.K.; Tripathi, D.K.; Avtar, R. Integrated Spatial Analysis of Forest Fire Susceptibility in the Indian Western Himalayas (IWH) Using Remote Sensing and GIS-Based Fuzzy AHP Approach. *Remote Sens.* **2023**, *15*, 4701. [\[CrossRef\]](#)
89. Campbell, M.J.; Dennison, P.E.; Thompson, M.P.; Butler, B.W. Assessing Potential Safety Zone Suitability Using a New Online Mapping Tool. *Fire* **2022**, *5*, 5. [\[CrossRef\]](#)
90. Debnath, P. A QGIS-Based Road Network Analysis for Sustainable Road Network Infrastructure: An Application to the Cachar District in Assam, India. *Infrastructures* **2022**, *7*, 114. [\[CrossRef\]](#)
91. Carrión-Mero, P.; Montalván-Burbano, N.; Herrera-Franco, G.; Domínguez-Granda, L.; Bravo-Montero, L.; Morante-Carballo, F. Research Trends in Groundwater and Stable Isotopes. *Water* **2022**, *14*, 3173. [\[CrossRef\]](#)

**Disclaimer/Publisher’s Note:** The statements, opinions and data contained in all publications are solely those of the individual author(s) and contributor(s) and not of MDPI and/or the editor(s). MDPI and/or the editor(s) disclaim responsibility for any injury to people or property resulting from any ideas, methods, instructions or products referred to in the content.